Catalysis Today 283 (2017) 89–103

Contents lists available at ScienceDirect

Catalysis Today

journal homepage: www.elsevier.com/locate/cattod

Exploring structure and reactivity of Cu sites in functionalized UiO-67 MOFs

Luca Braglia[a,b], Elisa Borfecchia[a,**], Lorenza Maddalena[a], Sigurd Øien[c], Kirill A. Lomachenko[b], Aram L. Bugaev[a,b], Silvia Bordiga[a,c], Alexander V. Soldatov[b], Karl Petter Lillerud[c], Carlo Lamberti[b,d,*]

[a] Department of Chemistry, NIS and INSTM Reference Centers, University of Turin, via Quarello 15, I-10135 Turin, Italy
[b] IRC "Smart Materials", Southern Federal University, Zorge Street 5, 344090 Rostov-on-Don, Russia
[c] inGAP Centre for Research Based Innovation, Dept. of Chemistry, University of Oslo, Oslo, Norway
[d] Department of Chemistry, CrisDi Centre for Crystallography, University of Turin, via Giuria 7, I-10125 Turin, Italy

ARTICLE INFO

Article history:
Received 23 November 2015
Received in revised form 18 January 2016
Accepted 12 February 2016
Available online 23 April 2016

Keywords:
Metal organic frameworks
UiO-67
Post-synthetic functionalization
Cu-catalysts
operando XAS
in situ FTIR

ABSTRACT

The exceptional thermal stability of the UiO-67/68-family MOFs makes them ideal candidates to explore post-synthetic functionalization routes aiming to the heterogenization of homogeneous catalysts. We previously demonstrated that a small fraction of the linkers in the UiO-67 MOF can be replaced by bipyridine-dicarboxylate (bpydc) moieties exhibiting metal-chelating ability and enabling the grafting of Pt(II) and Pt(IV) ions in the MOF framework [Chem. Mater., 27 (2015) 1042]. Herein, we investigate a novel Cu-functionalized UiO-67 MOF obtained by a simple synthesis method, consisting in contacting the bpydc-containing UiO-67-bpy MOF with a $CuCl_2$ dihydrate precursor. By combining *in situ* and *operando* XAS and FTIR spectroscopies, we assessed the successful incorporation of well-defined Cu complexes in the UiO-67 framework and explored local coordination geometry, redox properties and reactivity of the dominant Cu species formed in different conditions relevant to potential future applications in catalysis. EXAFS fits and XANES simulations, based on DFT-optimized geometries, yielded detailed structural and electronic information on the major Cu-species formed. Data analysis revealed three-coordinated Cu(I) complexes with the bpydc linker of the Cu-UiO-67 MOFs and a Cl^- ligand, formed after thermal treatment at 523 K in inert gas flow able to efficiently and reversibly form Cu(I)-mono-carbonyl adducts with CO adsorbate.

1. Introduction

Metal-organic Frameworks (MOFs) are defined as porous, crystalline materials composed by metal-based cornerstones (metal ions or clusters) connected by organic linkers [1–3] to form a three-dimensionally ordered framework. Due to their high surface area, and enormous structural and compositional flexibility, these micro-porous materials had attracted in the last decade a paramount research attention.

Our group have previously synthesized and thoroughly characterized the UiO-66, -67 and -68 classes of *iso*-structural MOFs, obtained by connecting $Zr_6O_4(OH)_4$ inorganic cornerstones with 1,4-benzene-dicarboxylate, 4,4′biphenyl-dicarboxylate and 4,4′-terphenyl-dicarboxylate linkers, for the UiO-66, −67 and −68 MOFs, respectively [4–9]. Due to their outstanding stability at high temperatures, high pressures and in presence of different solvents, these materials are among the few MOFs already commercialized for applications in the fields of catalysis, H_2 storage, and gas purification [1–3,6].

An additional key feature of MOFs is the possibility to easily tune their properties by post-synthetic functionalization (PSF) [10–12], acting either on the metal ions or on the linkers. Such approach yielded for instance to the incorporation of Au(III) Schiff base complexes onto type-IRMOF-3 MOFs previously grafted with salicylaldehyde molecules, obtaining a highly active and selective catalyst for three-dimensional coupling and cyclization reactions in the liquid phase [13]. PSF of the UMCM-1-NH_2 MOF also allowed

* Corresponding author at: IRC "Smart Materials", Southern Federal University, Rostov-on-Don, Russia and Department of Chemistry, CrisDi Centre for Crystallography, University of Turin, Turin, Italy.
** Corresponding author at: Department of Chemistry, NIS and INSTM Reference Centers, University of Turin, Turin, Italy.
E-mail addresses: elisa.borfecchia@unito.it (E. Borfecchia), carlo.lamberti@unito.it (C. Lamberti).

http://dx.doi.org/10.1016/j.cattod.2016.02.039
0920-5861/

Tanabe and Cohen to synthesize a series of Cu(II), Fe(III) and In(III) metallated derivatives. The resulting MOF-based catalysts are highly robust and active for epoxide ring-opening reactions [14]. Another remarkable example is the functionalization of the LSK-1 P-coordination polymer with Au(I) sites, yielding active and recyclable catalysts [15]. These materials were thoroughly characterized by NMR spectroscopy, TEM and Au L_3-edge high energy resolution XANES. The latter technique allowed the authors to rule out the formation of metal nanoparticles, confirming that Au is exclusively present in the form of Au(I) complexes. In addition, Bloch et al. recently reported a three-dimensional MOF particularly suited for post-synthetic metallation due to the presence of pore cavities lined with vacant di-pyrazole groups [16]. The potentialities of the Rh-functionalized derivative were demonstrated by capturing a series of single-crystal X-ray diffraction snapshots of the reaction products of consecutive oxidative addition and methyl migration steps occurring within the MOF pores.

The outstanding properties of the UiO-67/68-family MOFs make them an ideal test bench to explore PSF approaches [17–20], aiming to bridge the gap between homogeneous and heterogeneous catalysis. Indeed, a small fraction of the linkers in the UiO-67 MOF can be replaced by moieties exhibiting metal-chelating ability, such as bipyridine-dicarboxylate (bpydc), enabling the grafting of additional metal ions, while retaining the exceptional thermal and hydrothermal stability of the parent MOF. With this respect, we recently synthesized by different routes proof-of-concept Pt-functionalized UiO-67 derivatives [20]. Static and *operando* Pt L_3-edge XAS experiments allowed us to thoroughly characterize these materials and their rich reactivity, in the local environment of the Pt centers. Indeed, the Pt(II) complexes grafted to the MOF framework *via* the bpydc linker can be reduced to bpydcPt(0) sites under H_2 flow in the 600–700 K range, as probed by a sophisticated parametric analysis of temperature-dependent EXAFS data, or oxidized at room temperature to Pt(IV) through oxidative addition of Br_2 from the liquid phase. The large pore size of UiO-67 also allows for ligand exchange between $2Cl^-$ and even bulky ligands such as toluene-3,4-dithiol [20]. These studies pave the way to the exploration of a novel class of metal-functionalized MOFs, representing attractive candidates for industrial applications aiming to heterogenization of homogeneous catalytic reactions, with the advantages of metal recyclability and efficient catalyst/product separation in the spent catalyst.

In this context, herein we investigate a novel Cu-functionalized UiO-67 MOF by combining *in situ*/*operando* XAS and *in situ* FTIR spectroscopies, aiming to assess the successful incorporation of well-defined Cu complexes in the UiO-67 framework and explore local coordination geometry, redox properties and reactivity of the dominant Cu species formed in different conditions, relevant to potential future applications in catalysis. This material is obtained by a simple synthesis route, by contacting the bpydc-containing UiO-67-bpy MOF with a Cu-containing precursor.

The choice of Cu-based functionalization was driven by several factors including its lower cost with respect to noble metals, and its rich catalysis in "click chemistry" [21,22]. Furthermore, in recent years, Cu-species hosted in porous materials, primarily zeolites and zeotypes, are emerging as key candidates to tackle some of the most urgent societal challenges in term of pollution and sustainable development. For instance, Cu-zeolites, initially ZSM-5 and mordenite [23–32] and more recently small pore zeolites and zeotype such as SSZ-13 and SAPO-34 [33], have been shown to be active for low temperature conversion of methane to methanol. Moreover, the small-pore Cu-SSZ-13 zeolite is attracting a great attention due to its outstanding performances in NH_3-assisted selective catalytic reduction (SCR) of NO_x gases contained in the exhaust fumes from road transport and industrial plants [34–41]. Although the active species are still profoundly debated, well defined mono- or multinuclear Cu-complexes hosted in the zeolite cages are emerging as key players in the NH_3-SCR or direct methane oxidation catalysis. Unusual coordination modes (*e.g.* three-fold coordination) adopted in the confined space where the reaction occurs and versatile redox chemistry are often observed in these Cu-species, resembling in several aspects their outperforming biologic counterparts [42–44]. In the view of mild reaction conditions, the potentialities of MOFs, exhibiting a much larger diversity and flexibility in composition and less demanding topological constraints in the formation of the porous lattices [45,46], could be optimally exploited to design valid alternatives to zeolite-based matrixes.

Also of potential interest is the immobilization of $CuCl_2$ in the nitrogen containing polymers, such as poly(4-vinylpyridine) (P4VP) [47], for the oxidative carbonylation of methanol to dimethylcarbonate [48–50], the oxidative coupling of 2,6-dimethylphenol [51] and the oxidation of tetralin [52]. Moreover, such copper chloride complexes may be of interest also for the oxychlorination catalysis [53–60].

Generally speaking, coordination chemistry of transition metal ions confined in the cavities of nanoporous hosts, such as MOFs, zeolites, and polymeric scaffolds, is substantially different with respect to liquid phase homogeneous organometallic chemistry [12,29,61–63]. Metal complexes formed in such conditions will experience strongly reduced mobility with respect to the solution phase case, which limits deactivating aggregations. Furthermore, complexation with extra-framework ligands will compete with the platform of ligands offered by the hosting matrix (bpydc chelating moieties in the present case, or framework oxygens in zeolites). Depending on the relative coordination strengths and on the unique nano-environment around the metal center, unusual low-coordination number/low-symmetry complexes can be obtained, which most likely would never be synthesized in the solution phase. Considering also the coordinative flexibility of Cu-centers and the possibility to treat the materials *in situ* under controlled conditions, a novel cage-confined coordination chemistry is emerging, yielding size- and shape-constrained Cu-complexes stabilized *via* host-guest interactions, which possess the potential to surpass their homogeneous counterparts in catalytic activity and enantioselectivity.

This novel research area growing at the border between heterogeneous and homogeneous catalysis strongly requires *in situ* and *operando* multi-technique approaches ensuring both local and long-range sensitivity, to efficiently monitor both the metal centers and the hosting framework in catalysis-relevant conditions [64–69].

In the present work, we combined *operando* XAS, *in situ* FTIR spectroscopy and DFT modeling, to clarify the local coordination geometry and oxidation state of the Cu centers, while assessing the immobilization of redox-active Cu-species in the UiO-67 framework. The interpretation of the results was also guided by the comparison with a well-defined Cu molecular complex, *tert*-butylbipyridinedichlorocopper (II) (tBbpyCuCl_2), characterized in detail by single-crystal XRD and XAS. We observed three-coordinated Cu(I) complexes with the bpydc linker of the Cu-UiO-67 MOFs and one Cl^- ligand, formed after thermal treatment at 523 K in inert gas flow. The identification of these species, able to efficiently and reversibly form Cu(I)-mono-carbonyl adducts with CO molecule, pave the way to further *operando* studies, exploring for instance the effect of more powerful reducing agents (*e.g.* H_2) and the reactivity towards molecular oxygen, based on the analogies with T-shaped oxygen-activating copper enzymes encountered in literature [44].

2. Materials and Method

2.1. Samples preparation

The starting UiO-67-bpy MOFs were synthesized by standard solvothermal method, as described in more details in a previous study [20], by reacting $ZrCl_4$ with different mixtures of H_2bpdc and H_2bpydc linkers (5% wt., 10% wt. and 20% wt. of bpydc) in a solution of dimethylformamide (DMF). 5 Molar equivalents of benzoic acid were added to obtain a modulator effect, which resulted in a porous MOF with monodispersed particles and well-defined crystallinity [70]. The Cu-functionalized Cu-UiO-67-bpy derivatives were prepared employing a PSF approach, by submerging the MOF powder in solution of $CuCl_2$ dihydrate in 2-propanol, and heating the solution at reflux conditions for one hour. The resulting bright green powders were washed in three cycles with 2-propanol and dried at 60 °C in air for 12 h prior to measurement. The three corresponding final products analysed in the present study will be hereafter referred to as Cu-UiO-67-5%bpy, Cu-UiO-67-10%bpy, and Cu-UiO-67-20%bpy, respectively. The final Cu concentration in the samples has been evaluated from the edge jump of the corresponding XAS spectra and is: Cu-UiO-67-5%bpy: 0.9Cu%wt; Cu-UiO-67-10%bpy: 1.8Cu%wt; and Cu-UiO-67-20%bpy: 4.5Cu%wt.

tert-Butylbipyridinedichlorocopper (II) ($tBbpyCuCl_2$) was chosen as reference compound having both N and Cl atoms in the first coordination shell of Cu. It was prepared according to the method described by Awad et al. [71]. The crude compound was re-crystallized in a vapor diffusion setup using dichloromethane (DCM) as solvent and cyclohexane as antisolvent [72].

2.2. In situ and operando XAS experiments

Cu-K edge (8979 eV for Cu foil) XAS data were collected at the I811 beamline of the Max Lab II source (Lund, Sweden) [73]. Max Lab II was operating at 1.5 GeV with a uniform current between 250 and 100 mA. The white beam produced by a liquid He-cooled superconducting wiggler was monochromatized by a horizontally sagitally focused double-crystal Si(111) monochromator, detuned to 20% to minimize the third harmonic. Spectra were collected in transmission mode using 30 cm ionization chambers for I_0 and I_1 with N_2 and Ar gases to guarantee 17% and 74% of absorption, respectively [66,67]. The intensity I_2 transmitted by a Cu-reference foil located after the sample was measured using a photodiode, and the resulting spectrum was employed for energy alignment purpose.

XAS spectra of Cu-UiO-67 MOF samples were measured employing a home-made cell allowing sample activation in temperature and gas dosage under *in situ* or *operando* conditions [74], monitoring the evolution of the XAS features while controlling temperature and gas feed. The pure powdered Cu-UiO-67 MOF samples were pressed into self supporting pellets, which were then inserted in the cell. The weights of the pellets were optimized in order to obtain the best S/N ratio for XAS measurements in transmission mode ($\Delta\mu x$ in the 0.2–0.8 range, depending on Cu-loading, with estimated total absorption of $\mu x \sim 2.4$), resulting in 80–120 mg per 1.3 cm^2 pellets. After XAS characterization of the as-prepared MOFs, the samples were heated in N_2 until 523 K to remove residual solvent (DMF and 2-propanol) and water and explore the possibility to obtain coordinatively unsaturated Cu-sites by mild thermal treatment in inert atmosphere. After the heating ramp, the samples were cooled down to RT, always in N_2 flux. Subsequently, the gas feed was switched from N_2 to 40% CO in N_2, mixture to probe the reactivity of the thermally-treated material and achieve deeper insights in the nature of the Cu sites monitoring their interaction with the CO probe molecule. The samples were hence monitored by XAS after CO desorption at RT (by switching back the gas feed to N_2) and heating again to 523 K (always in N_2). The XAS data reduction and EXAFS extraction procedure was performed using the Athena code [75].

2.3. Computational details

Several local environments for Cu(II) and Cu(I) sites grafted to the UiO-67 framework by coordination to the bpydc linker were optimized at DFT level using Perdew-Burke-Ernzerhof (PBE) [76] exchange-correlation functional implemented in VASP 5.3 code [77,78]. Kinetic energy cutoff for the plane-wave basis set was set to 400 eV. The optimized environments include: [Cu(bpydc)Cl_2], [Cu(bpydc)(OH)Cl], [Cu(bpydc)Cl], [Cu(bpydc)(CO)Cl], and single CO molecule in the gas phase. A single k-point calculation in a periodic cell was performed for all of the structures. The DFT-optimized structures were employed as input geometries for XANES simulations (see Section 2.5). These also served as starting point for EXAFS fitting (see Section 2.4), to set coordination numbers and provide initial values for the bond distances of each coordination shell from the Cu absorber, to be then experimentally refined in the fitting procedure. Theoretical vibrational frequencies were calculated on the basis of the matrix of second derivatives obtained by numeric differentiation of forces. At this level of theory, the obtained CO bond length was equal to 1.14 Å, which is in agreement with the experimentally known 1.13 Å value [79], and the theoretical vibrational frequency was obtained at $\tilde{\nu}^{theo}(CO) = 2123\ cm^{-1}$, which is slightly underestimated with respect to the experimental value of $\tilde{\nu}^{exp}(CO) = 2143\ cm^{-1}$ [80]. For this reason, as usually accepted, the comparison between experimental and theoretical CO stretching frequencies will not be made on the absolute values ($\tilde{\nu}^{exp}(CO)$ and $\tilde{\nu}^{theo}(CO)$) but on the shifts: $\Delta\tilde{\nu}^{exp}(CO) = [\tilde{\nu}^{exp}(CO) - \tilde{\nu}_0^{exp}(CO)]$ and $\Delta\tilde{\nu}^{theo}(CO) = [\tilde{\nu}^{theo}(CO) - \tilde{\nu}_0^{theo}(CO)]$.

2.4. EXAFS fitting

The EXAFS spectra collected at RT for the as-prepared and N_2-thermally treated samples (Cu-UiO-67-5%bpy, -10%bpy and -20%bpy) were fitted in R-space in the $\Delta R = (1.0–4.8)$ Å range, considering the FT of the k^2-weigthed $\chi(k)$ EXAFS spectrum, Fourier transformed in the (2.5–12.0) $Å^{-1}$ range, potentially resulting in 23 independent parameters ($2\Delta k \Delta R/\pi > 23$). Phases and amplitudes were calculated by the FEFF6 code [81,82] using the Artemis software from the Demeter package [75] and checked on the $tBbpyCuCl_2$ model compound. In the fitting model, all the single scattering (SS) and multiple scattering (MS) paths contributing to the R-space interval of interest were included.

To limit the number of optimized variables, all the SS and MS paths calculated from each starting DFT-optimized geometry have been optimized with the same passive amplitude reduction factor (S_0^2) and with the same energy shift parameter (ΔE). In the fits of thermally-treated samples, and of the N_2-thermally treated + CO Cu-UiO-67-10%bpy sample, the S_0^2 values were set to the same best fit values refined for the corresponding as-prepared material.

The parameterization of the EXAFS paths was performed including all the first shell SS paths with specific ΔR and Debye Waller (DW, σ^2) parameters (including the SS involving the N(bpy), Cl, O(OH) and C(CO) atoms, depending on the specific experimental conditions considered). For the bpy unit, the SS paths for the three shells of C atoms (C_1 at *ca.* 2.92 Å, C_2 at *ca.* 4.30 Å and C_3 at *ca.* 4.81 Å) and the numerous, and rather intense, MS paths involving the N, C_1, C_2, and C_3 atoms were included in the fitting model with a "collective" parametrization strategy. More specifically, these paths were modeled considering a global contraction/expansion factor for the whole bpy unit α_{bpy} and a DW factor σ^2_{bpy} increasing as the square root of the distance $R_{eff,i}$ of the i^{th} scattering atom from the absorber ($\Delta R_{bpy,i} = \alpha_{bpy}\ R_{eff,i}$, $\sigma^2_{bpy,i} = \sigma^2_{bpy}\ (R_{eff,i}/R_0)^{1/2}$, being $R_0 = 2.026$ Å;

resulting in only two optimized parameters: α_{bpy}, σ^2_{bpy}), as already successfully tested in EXAFS analysis involving complex multi-atomic ligands/coordination environments [40,83–86].

2.5. XANES simulations

The XANES spectra were simulated by the new sped-up version of the FDMNES code [87], employing the finite-difference method to solve the Schrödinger equation [88,89]. The energy-dependent exchange-correlation potential was obtained following the Hedin and Lundquist formulation. In order to match the spectral resolution observed in the experiment, energy-dependent broadening was applied. Importantly, we performed self-consistent calculations without imposing any restriction to the shape of the potential [89]. The latter has been previously demonstrated to yield very good agreement with the experimental data for molecules [90] and structures with cavities and channels [87].

2.6. FTIR in situ characterization

In situ FTIR spectra were recorded in transmission mode on a Bruker VERTEX 70 FTIR spectrometer, equipped with an HgCdTe (MCT) cryo-detector using a home-made cell allowing sample activation in temperature under dynamic vacuum down to 10^{-4} Torr, precise dosage of the desired equilibrium pressure of a given probe molecule and cooling down to liquid-nitrogen temperature. FTIR data for the as-prepared and N_2-thermally-treated samples, in the form of pure thin self-supported pellets (no optical diluent has been used), were recorded at RT. Interaction with CO was performed at *ca.* 100 K dosing an equilibrium pressure of 30 Torr. Lower CO equilibrium pressures were investigated down to 10^{-3} Torr by progressive expansions in a dead volume that can be successively evacuated. Each spectrum has been obtained averaging 32 interferograms, recorded at 2 cm^{-1} resolution. A detailed scheme of the *in situ* IR cells available at the NIS laboratories of the Turin University has been reported in the ESI of Ref. [91] (Fig. S4).

2.7. Single-crystal XRD on tBbpyCuCl$_2$ model compound

From the batch of tBbpyCuCl$_2$ synthesized crystals, a suitable crystal was chosen for single-crystal X-ray diffraction and measured at 100 K using a Bruker D8 Venture diffractometer equipped with a Mo anode (MoKα: λ = 0.71073 Å). The data reduction was performed with Bruker SAINT and SADABS, and the structure was solved with XT and refined with XL [92]. Olex2 [93], Diamond [94] and Encifer [95] were used to create illustrations and cif files.

3. Results and discussion

3.1. Structural characterization of the tBbpyCuCl$_2$ model compound

The comparison between Cu-UiO-67-bpy MOFs and well-defined molecular Cu-bpyridine complexes is an important step to assess the success of the PSF process, and to gather information on the coordination environment and oxidation state of Cu-sites in the as-prepared samples. For these reasons, multiple attempts were made to synthesize complexes of Cu(II) with two Cl ligands and either 2,2′-bipyridine (bpy) or H_2bpydc as ligands, to be used as reference compounds for the XAS measurements. However, these were difficult to procure in the required quantity and purity, and the product was a mixture of polymorphs, or dimeric species as previously reported [96]. Another reference compound based on *tert*-butylbipyridine (tBbpyCuCl$_2$) was hence chosen, and prepared as described in Section 2.1. This resulted in a pure crystalline product suitable for single-crystal XRD characterization and XAS measurements.

Details on the single-crystal XRD data collection and structure refinement are reported in Table S1 of the Supporting information, while the refined structure of the tBbpyCuCl$_2$ complex is reported in Fig. 1a. For each atom, the corresponding anisotropic atomic displacement parameters (at 100 K) are represented with ellipsoids. The resulting crystal structure has been submitted to CCDC with number 1445442.

The output of the XRD refinement was used as input for the EXAFS data analysis in order to check the validity of the theoretical Cu–N and Cu–Cl phases and amplitudes generated by FEFF6 code [81,82]. As reported in Fig. 1b,c, the quality of the EXAFS fit was excellent, and the numerical output was in perfect agreement with the distances obtained from XRD. Fixing the coordination numbers to the values $N_N = N_{Cl} = 2$, reasonable values have been obtained for both the passive amplitude reduction factor ($S_0^2 = (0.94 \pm 0.02)$, expected to be close to unit) and for the DW parameters ($\sigma^2_{N(bpy)}$ and σ^2_{Cl}), see Table 1. This structural check guarantees that reliable quantitative results can be achieved from the EXAFS analysis of the Cu-functionalized UiO-67 MOF sample measured in different conditions.

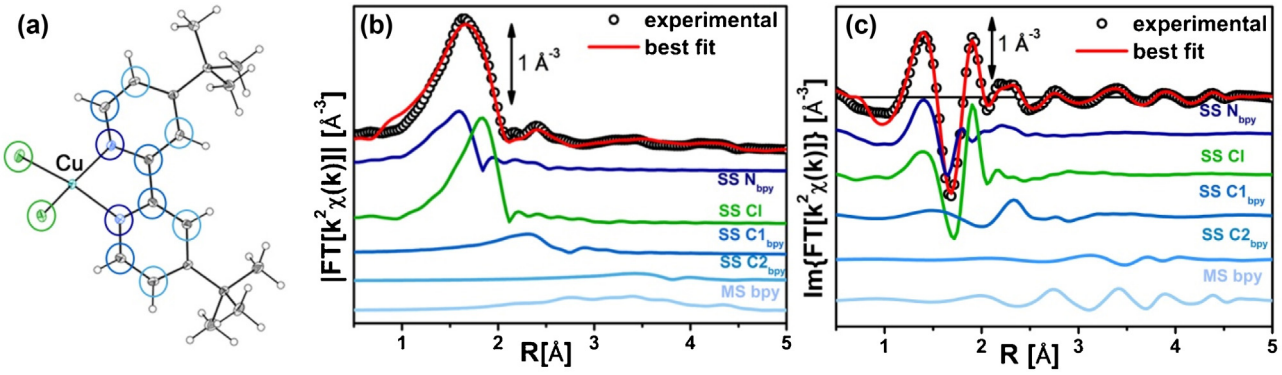

Fig. 1. Part (a): structure of the tBbpyCuCl$_2$ model compound as obtained from the single-crystal XRD refinement (data collected at 100 K). Atoms are represents as ellipsoids according to the refined thermal displacement parameters. The colored circles around the atoms refer to the different paths used in the EXAFS data analysis. Part (b): comparison between experimental (empty circles) and best fit (red line) of the k^2-weighted, phase uncorrected modulus of the Fourier transformed (FT) EXAFS spectrum of the tBbpyCuCl$_2$ model compound, measured at RT. The different paths included in the fit are also reported, with the same color code as the circles in part (a), and vertically translated for clarity. Part (c): as part (b) for the corresponding imaginary parts of k^2-weighted, phase uncorrected FT EXAFS spectrum of the tBbpyCuCl$_2$ model compound. (For interpretation of the references to color in this figure legend, the reader is referred to the web version of this article.)

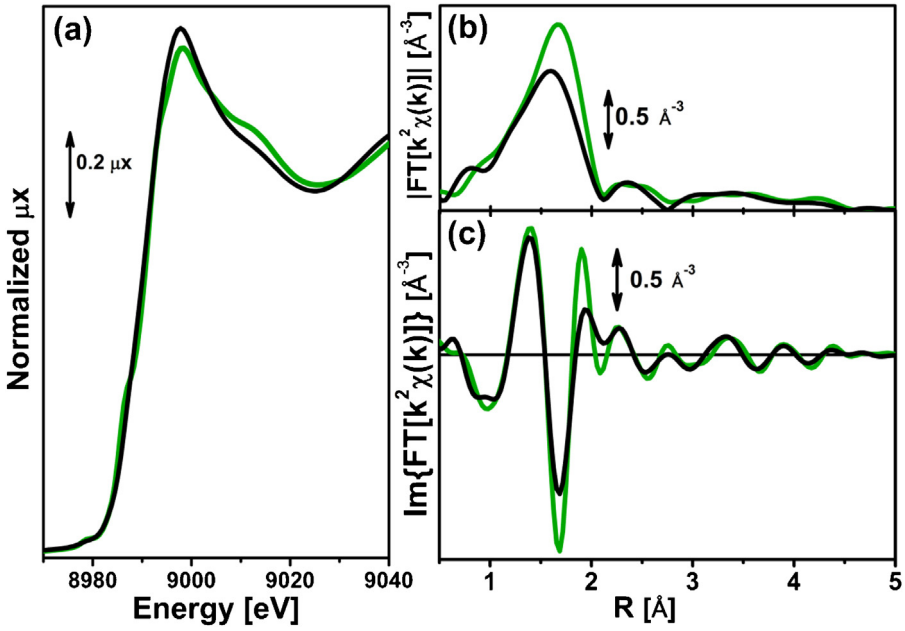

Fig. 2. Part (a): Cu K-edge XANES spectra of Cu-UiO-67-10%bpy (black) and of tBbpyCuCl$_2$ model compound (green) collected at RT in air. Parts (b, c): Moduli (b) and imaginary parts (c) of the k^2-weighted, phase uncorrected, FT EXAFS spectra collected in the same experimental conditions reported in part (a), using the same color code. (For interpretation of the references to color in this figure legend, the reader is referred to the web version of this article.)

Table 1
Best-fit values of the parameters optimized in the EXAFS fits for the tBbpyCuCl$_2$ model compound, performed in the k-space interval $\Delta k = (2.5–17.0)\,Å^{-1}$ and R-space interval $\Delta R = (1.0–5.0)$ Å, potentially resulting in 36 independent parameters ($2\Delta k \Delta R/\pi > 36$). Average bond distances from the Cu-absorber for the first shell ligands refined from single-crystal XRD are also reported in the last column, for comparison.

EXAFS fit parameters	EXAFS	Single-crystal XRD
$S_0{}^2$	0.94 ± 0.02	–
ΔE (eV)	0.6 ± 0.2	–
R-factor	0.011	–
N_{par} (N_{ind})	8 (36)	–
$<R_{N(bpy)}>$ (Å)	1.990 ± 0.003	1.995
$\sigma^2{}_{N(bpy)}$ (Å^2)	0.0021 ± 0.0005	–
$N_{N(bpy)}$	2	
α_{bpy}	-0.004 ± 0.003	–
$\sigma^2{}_{bpy}$ (Å^2)	0.0021 ± 0.0005	–
$<R_{Cl}>$ (Å)	2.217 ± 0.003	2.218
$\sigma^2{}_{Cl}$ (Å^2)	0.0032 ± 0.0003	–
N_{Cl}	2	

3.2. *As-prepared and thermally-treated Cu(II)-UiO-67 and comparison with tBbpyCuCl$_2$ model compound: XAS experimental evidences*

At the first step, the XAS experiments were carried out at RT in air, to verify the successful grafting of the metal centers in the UiO-67 framework and investigate the dominant local environment for Cu-sites in the as-prepared samples. Subsequently, *operando* experiments allowed us to monitor the evolution of the spectral features while heating from RT up to 523 K in N_2 flow. After the thermal treatment, the sample has been cooled down at RT, and further characterized by *in situ* XAS. This characterization protocol was repeated for all the three selected samples of Cu-UiO-67-bpy characterized by different concentration of bpydc linkers: Cu-UiO-67-5%bpy, -10%bpy and -20%bpy, to assess the effect of the functionalization level on Cu-speciation in the different experimental conditions probed.

A first simple comparison of the XANES (Fig. 2a) and EXAFS (Fig. 2b,c) data collected on as-prepared Cu-UiO-67-10%bpy in air (black) and on the tBbpyCuCl$_2$ model compound (green) clearly testifies that the Cu-UiO-67-10%bpy sample hosts a large majority of Cu (II) species. However, the local environment of Cu atoms in the two materials is significantly different. This case differs from what observed for the functionalization of UiO-67 with Pt(II), where the local environment of Pt was the same in the bpydcPtCl$_2$ linker and in the MOF [20]. Indeed, the EXAFS data clearly shows a lack of EXAFS signal in the (1.5–2.1) Å region in Cu-UiO-67-10%bpy, suggesting the presence of only one Cl atom in the first coordination shell of the copper atoms (Fig. 2b,c). Moreover, the loss of spectroscopic definition of the features of the XANES spectrum of Cu-UiO-67-10%bpy (Fig. 2a) suggest an increased heterogeneity of Cu environment. Consequently the EXAFS data analysis on the Cu functionalized MOFs cannot be performed by a straightforward duplication of the refinement strategy adopted for the tBbpyCuCl$_2$ model compound and will require some additional attention (see Section 3.3). Fig. 3 reports the XANES spectra (part a) and the k^2-weighted, phase uncorrected (parts b,c), Fourier transformed EXAFS spectra for the exemplificative case of Cu-UiO-67-10%bpy during the thermal treatment in inert gas flow, from RT (as-prepared state, black lines) to 523 K (purple line). XANES spectra for intermediate temperatures are also reported, as gray thin lines in part (a).

The XANES spectrum for the as-prepared material is characterized by the absence of any defined pre-edge/edge peaks, and by a rather intense white line feature at ~8996.6 eV, typical of Cu(II) centres coordinated to water molecules and, eventually, OH groups [32,39,97–99]. As also supported by the comparison with the tBbpyCuCl$_2$ model compound, the overall shape and the edge energy position in the XANES of the as-prepared material are consistent with a large majority of Cu(II) sites. The spectral changes observed during thermal activation involve a clear decrease of the white line feature, accompanied by a significant shift of the absorption edge towards lower energies (*ca.* 3.6 eV, as evaluated by monitoring the energy position of the first main maximum of the first derivative spectra [57,58], see Supporting information, Fig. S1). At the end of the heating ramp, a shoulder starts to be distinguishable in the XANES edge-rising region at *ca.* 8983 eV, falling in

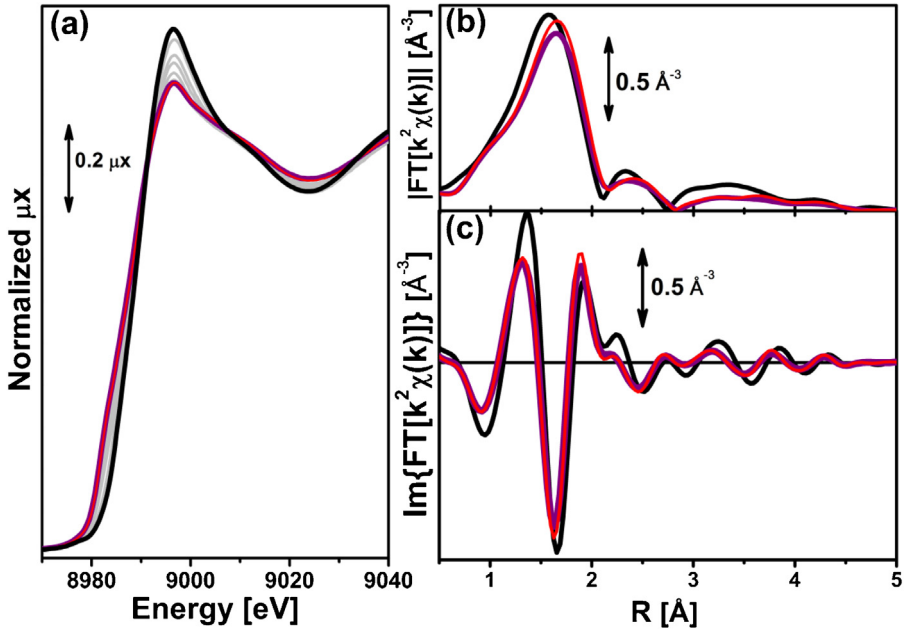

Fig. 3. Part (a): Cu K-edge XANES spectra of Cu-UiO-67-10%bpy during the temperature activation: at RT in air (black), at 523 K in N_2 flux (purple), at RT in N_2 after thermal treatment (red); grey spectra refer to intermediate temperatures. Parts (b, c): moduli (b) and imaginary parts (c) of the k^2-weighted, phase uncorrected, FT EXAFS spectra for the same experimental conditions reported in part (a), with the same color code. Intermediate spectra were omitted for clarity. (For interpretation of the references to color in this figure legend, the reader is referred to the web version of this article.)

an energy range typical for two- or three-coordinated Cu(I) sites [100,101].

These evidences suggest a ligand loss process associated to the reduction of a significant percentage of the starting Cu(II) sites to Cu(I), as thermal treatment proceeds [57–59,102]. Unfortunately the energy resolution of the present dataset was not sufficient to effectively monitor the weak pre-edge peak at *ca.* 8976.2 eV, which however can be distinguished only in the XANES of the as-prepared material and better located in energy by observing the first derivative spectrum (Supporting information, Fig. S1). Indeed, this peak mostly derives from the dipole-forbidden $1s \rightarrow 3d$ transition and it is commonly employed to fingerprint the presence of Cu(II) sites in the probed sample [24,39,40,100,101,103]. Nonetheless, the other spectral modifications, also accompanied by the sample color change from green to light-green/white as the temperature increases, support the formation of coordinatively unsaturated Cu(I) sites after mild thermal treatment in inert atmosphere.

The EXAFS spectra reported in Fig. 3b,c shows a small but significant decrease in the first shell intensity (in addition to the signal damping due to increased thermal contributions to DWs, see below), accompanied by a clear shift towards higher R-values. DFT-assisted analysis of the EXAFS spectra for as-prepared and thermally-treated samples allowed us to achieve deeper insights in the ligands environment of Cu-sites, and it will be discussed in the following (see Section 3.3). As expected, the XANES spectra collected on the thermally-treated sample at 523 K (purple line in Fig. 1) and after cooling down at RT, always in N_2 flux (red lines in Fig. 3) are fully equivalent. As, contrarily to EXAFS, XANES is almost unaffected by acquisition temperature, the equivalence of the XANES spectra collected at 523 K and at RT after thermal treatment indicates that no changes in the averaged local environment of Cu metal sites occur during the cooling process. Correspondently, EXAFS spectra show only slight differences in intensity, fully ascribable to the decreased thermal contribution to the DWs factors once cooled down to RT. This allowed us to perform quantitative EXAFS analysis on the spectrum collected at RT after N_2-thermal treatment, ensuring a higher data quality and an easiest comparison with the results obtained on the as-prepared material.

For both the as-prepared condition and after thermal treatment in N_2, the Cu-UiO-67-5%bpy, Cu-UiO-67-10%bpy, and Cu-UiO-67-20%bpy resulted in very similar XANES and EXAFS spectra, showing an equivalent evolution trend during the heating ramp (see Supporting information, Figs. S2 and S3). The strong similarity of the XAS features suggests that the same dominant Cu-species are formed irrespectively of the functionalization level. The small differences observed in the three samples will be further discussed in the following, in the view of the most likely coordinative environments proposed for Cu sites in the as-prepared materials and after heating in N_2 flux on the basis of DFT-assisted EXAFS fitting.

3.3. *DFT-assisted EXAFS analysis of as-prepared and thermally treated Cu-UiO-67-bpy*

The natural starting point in our study is the quantitative investigation of the local environment of Cu centers in the as-prepared material, to assess the successful immobilization of single Cu sites in the UiO-67-bpy MOF by exploiting the chelating capability of the bpydc linker. On the basis of XANES qualitative analysis, we could envisage four-coordinated planar Cu(II) sites. Staring from the $CuCl_2 \cdot 2H_2O$ precursor, this could be firstly realized by coordinating two N atoms from the bpydc linker and two Cl^- ligands. This model is however not supported by the comparison with the EXAFs signal of the tBbpyCuCl$_2$ model compound (Fig. 2b,c). To definitively rule out this model, the resulting expected [Cu(II)(bpydc)Cl$_2$] complex has been DFT-optimized and tested for the EXAFS fit of the as-prepared materials. Very interestingly, the fits resulted in rather high values for the DWs associated to the Cu–N(bpy) bond ($\sigma^2_{N(bpy)} \sim 0.004$ Å^2) and very high values for the DW associated to the Cu–Cl bonds ($\sigma^2_{Cl} \sim 0.007$ Å^2), which are definitely not reliable for RT data collection, and strongly discourage the coordination of two Cl ligands in a majority of Cu sites. Although inadequate to reproduce the first shell contribution, the fit revealed that the EXAFS signal in the (2.8–4.8) Å R-range is very

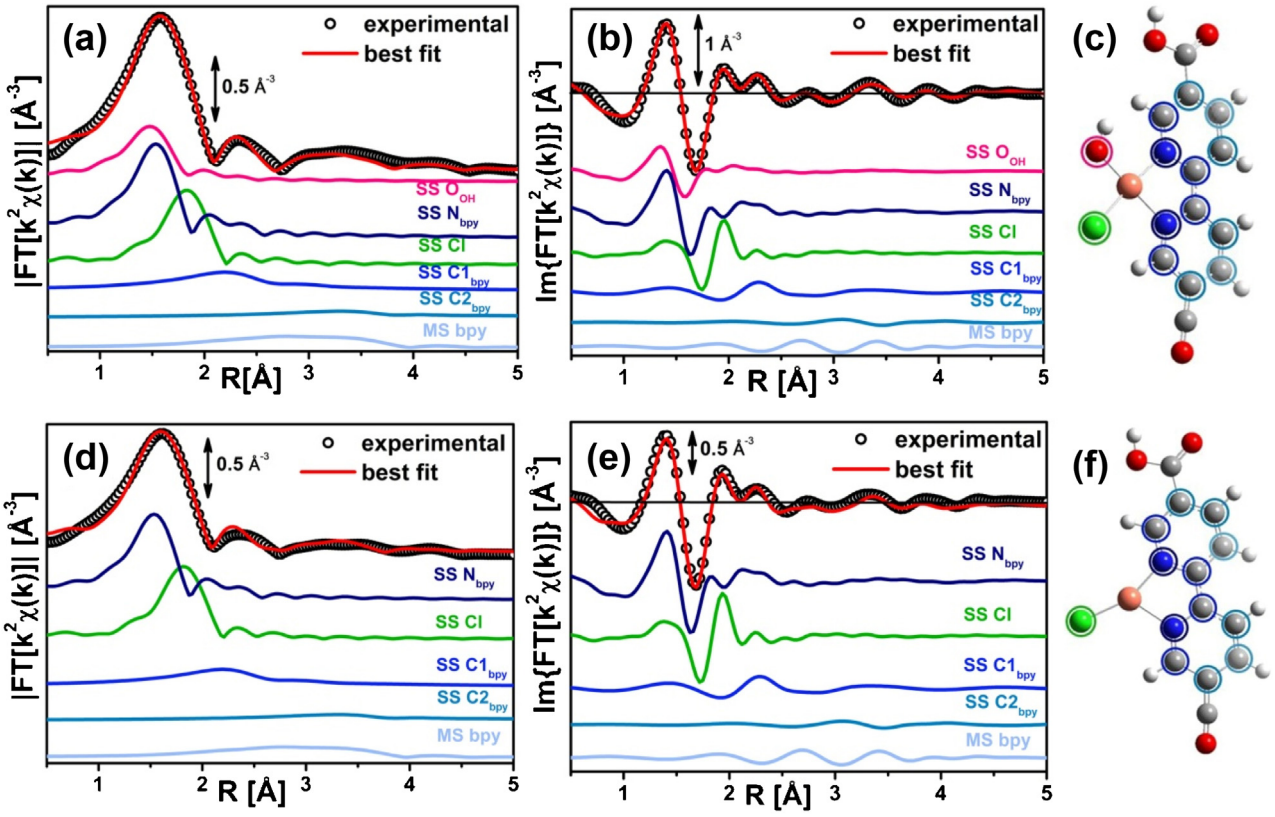

Fig. 4. Parts (a,b): k_2-weighted, phase uncorrected, modulus (a) and imaginary part (b) of the experimental and best fit FT EXAFS spectra for Cu-UiO-67-10%bpy in the as-prepared state (at RT, in air). The experimental data are shown as black dots and the best fit with red solid line. Moreover, the single scattering (SS) contribution involving the N(bpy), Cl, O(OH), C1(bpy) and C2(bpy) atomic neighbors as well as the multiple scattering (MS) involving the atoms of the bpy unit are reported. Part (c): DFT-optimized structure used as starting point for the EXAFS fit. Atom color code: Cu: orange; O: red; N: blue; Cl: green, C: gray; H: white. Parts (d, e, f): as parts (a, b, c) for the UiO-67-10%bpy-Cu(I) sample measured at RT after thermal treatment at 523 K in N_2. In parts (c, f), circled atoms are those included in the EXAFS fit and the color of the circle is the same used in parts (a, b, d, e) for the lines of the corresponding SS paths. (For interpretation of the references to color in this figure legend, the reader is referred to the web version of this article.)

well reproduced considering the numerous SS and MS [104–106] contributions from the bpydc unit (see below), thus allowing us to safely state that a successful chelation of the metal occurred during the PSF process. We thus considered the possible substitution of one Cl^- ligand with an OH^- group in the first coordination shell of Cu, yielding to the [Cu(II)(bpydc)(OH)Cl] complex. This new model is able to qualitatively explain the important differences observed in the EXAFS spectrum of the Cu-UiO-67-10%bpy MOF with respect to that of the tBbpyCuCl$_2$ model compound (Fig. 2b,c). It is worth to note that by EXAFS is almost impossible to distinguish coordination of O(H_2O) and O(OH) ligands, due to the weak scattering amplitude of H. However, the presence of a negatively charged hydroxyl group would allow to charge-balance Cu(II) sites, in agreement with the XANES signatures of the as-prepared materials. The relative DFT-optimized geometry is reported in Fig. 4c, foreseeing the following first-shell bond distances: Cu–O(OH) ~ 1.84 Å, <Cu–N(bpy)> ~ 2.01 Å and Cu–Cl ~ 2.21 Å. The [Cu(II)(bpydc)(OH)Cl] structure allowed to satisfactorily fit the EXAFS spectra for all the as-prepared Cu-UiO-67 samples, with good R-factor values and significantly more reliable DWs values with respect to the configuration with two chlorine ligands. As an example, Fig. 4a,b show the experimental modulus and imaginary part of FT for as-prepared Cu-UiO-67-10%bpy compared with the corresponding best fit curve. The figure also reports the principal scattering contributions to the global EXAFS signal, allowing for instance to appreciate how the signal from *ca.* 2.8 Å mostly arises from the bpydc unit contributions, with a major role played by the numerous MS paths involving the N, C_1 and C_2 shells of the chelating linker [104–106].

The best fit parameters for the whole sample series (Cu-UiO-67-5%bpy, -10%bpy, and -20%bpy) are reported in Table 2. As expected from the similarity between the experimental spectra (see Fig. S2 in the SI), the best-fit values found from the EXAFS fits are generally equivalent within their experimental errors. Moreover, all distance are in reasonable agreement with those obtained from DFT calculation (reported in the last column of Table 2) and used as starting guess of the fits.

Although in principle the distinction between the two subshells of N(bpy) and O(OH) scatterers is not straightforward, dealing with low-Z, almost isoelectronic neighbors, a test EXAFS fit on the as-prepared material performed using the [Cu(I)(bpydc)Cl] geometry yielded an unphysically low DW factor for the N(bpy) shell, $\sigma^2_{N(bpy)} = (0.0002 \pm 0.0008)\,Å^2$. Such inconsistency clearly testifies a lack of scattering contribution in the low-R region of the spectrum, which is partially compensated by an artificial enhancement of the N(bpy) SS paths. Also, the fit resulted in a significantly poorer reproduction of the experimental spectrum (R-factor = 0.03), supporting that the presence of an independent O(OH) contribution at slightly shorter distance, and characterized by higher mobility (*i.e.* higher DW) with respect to the N(bpy) ones allows a more appropriated description of the average coordination environment of the Cu sites in the as-prepared Cu-UiO-67-bpy MOF series.

However, the [Cu(I)(bpydc)Cl] model ensured a good fit of the final EXAFS spectra collected at the end of the N_2-thermal treatment, after cooling down to RT. The fit quality and the different

contributions to EXAFS signal for the exemplificative case of the Cu-UiO-67-10%bpy sample can be observed in Fig. 4d,e, while the correspondent three-coordinated DFT-optimized geometry is reported in part (f). Looking at the best fit values for the parameters optimized in the fit (Table 2, bottom part) an average slight shortening of the first shell bond lengths is observed for the whole sample series with respect to the as-prepared material, as expected when a first-shell ligand is lost. The structural parameters derived for Cu-UiO-67-5%bpy, -10%bpy and -20%bpy samples after thermal treatment in N_2 are globally equivalent within their experimental errors, pointing out also in this case the presence of the same major Cu-species irrespectively of the functionalization level.

A plausible scenario, able to consistently describe the evolution in both XANES and EXAFS spectra observed in *operando* conditions while heating in N_2, could thus involve: (i) the simultaneous presence of a more labile, low-atomic-number ligand (in our hypothesis an OH^- group) and a more strongly bonded Cl^- one in the first coordination sphere of Cu sites at ambient conditions; (ii) the preferential release of the negatively-charged OH^- ligand, triggering a reduction effect of the original four-coordinated Cu(II) sites to three-coordinated Cu(I) species, while preserving coordination to the UiO-67 framework by the chelating bpydc linker. Interestingly, a similar mechanism, relying on the cleavage of a Cu–$(OH)^-$ bond during thermal treatment in vacuum or inert gas flow, has been recently suggested to rationalize the so called "self-reduction" process in Cu-exchanged zeolites [40,97,98].

However, for the Cu-UiO-67-5%bpy and -20%bpy samples a slight lowering of the DWs associated to both Cu–N(bpy) and Cu–Cl is observed. This is also accompanied by a slight lowering in the fit quality, as evidenced by the higher R-factor values obtained in these cases. In this picture, the decreased first-shell DWs values for the Cu-UiO-67-5%bpy and -20%bpy samples after thermal treatment in inert gas flow (see Table 2, bottom part) could be explained with the presence of residual [Cu(II)(bpydc)(OH)Cl] species, representing a minor but still observable contribution to the EXAFS signal (averaged on all Cu-sites, weighting by their relative abundance). In these cases, the lack of the SS and MS paths arising from the (OH^-) ligand in a few Cu-sites could have been compensated by a slight enhancement of the contributions from N(bpy) neighbor, resulting in lower DWs. Interestingly, also looking at the XANES spectra for the three Cu-MOFs heated at 523 K (see Fig. S3 in the SI), small differences can be appreciated. In particular, a slightly less developed final state is observed for the Cu-UiO-67-5%bpy and -20%bpy samples, with respect to the Cu-UiO-67-10%bpy one. Nonetheless, due to the small entity of such differences, we can infer that they can be most likely connected to small fluctuations in the experimental conditions during thermal treatment.

Similarly, the as-prepared Cu-UiO-5%bpy sample (Fig. S2) seems to show already at ambient condition a minor contribution from '(OH^-)-deficient' Cu(I) environments, as suggested by small differences in the white line intensity, edge position and first-shell EXAFS intensity/position with respect to the Cu-UiO-67-10%bpy and -20%bpy samples. It is however important to underline that most of the EXAFS parameters refined for the low and high Cu-loading samples are equivalent within their experimental errors. Hence, possible deviations should concern no more than 10% of the overall Cu sites: for the large majority of the copper atoms the general picture described in Fig. 4c,f holds, irrespectively of Cu-loading (Table 2).

3.4. Reactivity of N_2-thermally-treated material towards CO: XAS analysis

The thermally-treated Cu-UiO-67-bpy10% sample was selected to further investigate the nature and reactivity of coordinatively unsaturated Cu(I) sites suggested on the basis of XAS analysis, which represent an attractive platform for possible applications in catalysis, as discussed in the introduction. To this aim, we exposed the material to a 40% CO in N_2 gas flow, at RT, while collecting XAS data. Intuitively, interaction of CO with [Cu(I)(bpydc)Cl] complexes is expected to result in [Cu(I)(bpydc)(CO)Cl], with the insertion of CO in the first coordination shell of Cu(I), as already observed for other metals [105]. Small but significant modifications were detected in such conditions, which can be observed in Fig. 5, both in the XANES, part (a), and in the EXAFS region, parts (b,c). In particular, in the XANES spectrum we observed a lowering of the shoulder at *ca.* 8983 eV, characteristic of the thermally-treated sample, and related in previous studies to three- or two-coordinated Cu(I) sites [100,101]. A rather flat edge rise is observed, supporting the coordination of the CO molecule to Cu sites, with the consequent restoration of a pseudo square-planar ligands environment. This is however not accompanied by a significant shift of the absorption edge, suggesting that the copper oxidation state is preserved during interaction with CO, consistently with FTIR evidences discussed below, see Section 3.6.

Qualitative comparison between the EXAFS spectrum collected upon interaction with CO and the one previously discussed for the thermally-treated material reveals a lowering in the first shell intensity, which is rather surprising if CO coordination to the Cu(I) centre is considered. Nonetheless, apart from the intensity lowering in the $|FT[k^2\chi(k)]|$ spectrum (Fig. 5b), a significant shift of the maxima and minima in the $Im\{FT[k^2\chi(k)]\}$ curve (Fig. 5c) can be appreciated, together with relevant modifications in the overall spectral shape in the (1.5–2.5) Å R-range. This peculiar behavior will be further examined below by DFT-assisted EXAFS fitting, showing that the experimental EXAFS signal is compatible with CO coordination to Cu(I) sites. Noteworthy, once that the gas flow is switched back to N_2 after interaction with CO, the XAS features characteristic of the thermally-treated material are partially restored already at RT, while heating to 523 K the XANES and EXAFS signatures associated to the [Cu(I)(bpydc)Cl] sites were fully restored (see light blue line in Fig. 5), testifying the complete desorption of CO ligands.

The peculiar EXAFS features observed for the material in interaction with CO are consistent with a destructive interference between the additional EXAFS paths arising when CO is added in the Cu coordination sphere and the other contributions assigned to N(bpy) and Cl ligands. Indeed, for suitable Cu–(CO) bond lengths, such antiphase effect would result in a 'counterintuitive' lowering in the first shell peak intensity in the $|FT[k^2\chi(k)]|$ curves before and after the interaction of the thermally-treated material with CO, although moving from threefold to fourfold coordinated Cu centers. To further explore this possibility, we DFT-optimized the [Cu(I)(bpydc)(CO)Cl] complex, aiming to reproduce the local environment of Cu-carbonyl complexes formed in the experimentally probed conditions. The resulting optimized geometry is reported in Fig. 6c (DFT bond distances: Cu–C(CO) ~ 1.96 Å, <Cu–N(bpy)> ~ 2.01 Å, Cu–Cl ~ 2.20 Å), and it was employed to fit the EXAFS spectrum collected for the Cu-UiO-67-10%bpy sample after interaction with CO at RT. The best fit and experimental spectra are compared in Fig. 6a,b, which reports also the major SS and MS contributions to the EXAFS signal. The employed structure ensured a good reproduction of the experimental spectrum, with physically reliable optimized parameters values (see Table 3). The contribution of a group of rather intense (almost-collinear) MS involving the atoms of the CO ligand (pink curve in Fig. 6b), results in a mutual signal cancellation between the contribution associated to CO and the ones deriving from bpy and Cl ligands, justifying the experimentally observed damping in the first shell intensity. As expected, the interaction with CO promotes a global increase in the static disorder in the Cu local environment, as testified by a global slight increase of the DW factors with respect to the thermally-treated state, which however are still optimized to

Table 2
Best-fit values of the parameters optimized in the EXAFS fits for the three samples (5%bpy, 10%bpy and 20%bpy) in the as-prepared state (upper part) and after thermal treatment in N_2-flow at 523 K (lower part, data collected at RT). The fits were performed in the k-space interval $\Delta k = (2.5–12.0)\,Å^{-1}$ and R-space interval $\Delta R = (1.0–4.8)\,Å$, potentially resulting in 23 independent parameters ($2\Delta k \Delta R/\pi > 23$). The underlined parameters were fixed in the fit and have no associated error. DFT-optimized bond distances from the Cu-absorber for the first shell ligands are also reported in the last column, for comparison.

EXAFS fit parameters	As-prepared (RT, air)			DFT-opt. distances [Cu(II)(bpy)Cl(OH)]
	Cu-UiO-67-bpy5%	Cu-UiO-67-bpy10%	Cu-UiO-67-bpy20%	
S_0^2	0.93 ± 0.04	0.93 ± 0.03	0.92 ± 0.03	–
ΔE (eV)	2.3 ± 0.6	1.7 ± 0.6	1.6 ± 0.6	–
R-factor	0.008	0.009	0.008	–
N_{par} (N_{ind})	10 (23)	10 (23)	10 (23)	
$R_{O(OH)}$ (Å)	1.91 ± 0.01	1.91 ± 0.01	1.92 ± 0.01	1.84
$\sigma^2_{O(OH)}$ (Å^2)	0.004 ± 0.002	0.004 ± 0.002	0.004 ± 0.001	–
$<R_{N(bpy)}>$ (Å)	2.024 ± 0.006	2.026 ± 0.006	2.026 ± 0.005	2.01
$\sigma^2_{N(bpy)}$ (Å^2)	0.003 ± 0.001	0.0023 ± 0.0006	0.0023 ± 0.0006	–
α_{bpy}	-0.004 ± 0.008	-0.010 ± 0.005	-0.011 ± 0.005	–
σ^2_{bpy} (Å^2)	0.009 ± 0.002	0.006 ± 0.001	0.006 ± 0.001	–
R_{Cl} (Å)	2.253 ± 0.006	2.265 ± 0.006	2.269 ± 0.006	2.21
σ^2_{Cl} (Å^2)	0.0036 ± 0.0007	0.0038 ± 0.0007	0.0040 ± 0.0007	–
EXAFS fit parameters	After thermal treatment at 523 K in N_2 (measured at RT)			DFT-opt. distances [CuI(bpy)Cl]
	Cu-UiO-67-bpy5%	Cu-UiO-67-bpy10%	Cu-UiO-67-bpy20%	
S_0^2	0.93	0.93	0.92	–
ΔE (eV)	1.6 ± 0.8	2 ± 1	2.3 ± 0.8	–
R-factor	0.014	0.011	0.015	–
N_{par} (N_{ind})	7 (23)	7 (23)	7 (23)	–
$<R_{N(bpy)}>$ (Å)	1.985 ± 0.008	1.989 ± 0.008	1.995 ± 0.008	2.00
$\sigma^2_{N(bpy)}$ (Å^2)	0.0021 ± 0.0006	0.0026 ± 0.0007	0.002 ± 0.001	–
α_{bpy}	-0.018 ± 0.012	-0.015 ± 0.009	-0.012 ± 0.008	–
σ^2_{bpy} (Å^2)	0.011 ± 0.003	0.009 ± 0.003	0.008 ± 0.002	–
R_{Cl} (Å)	2.249 ± 0.007	2.249 ± 0.007	2.258 ± 0.007	2.29
σ^2_{Cl} (Å^2)	0.0030 ± 0.0006	0.0034 ± 0.0006	0.0026 ± 0.0006	–

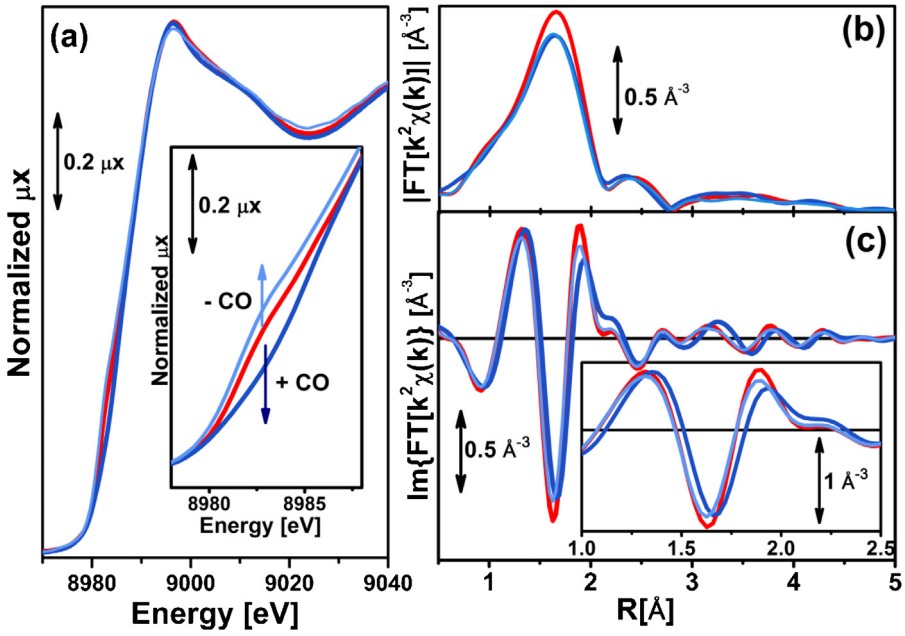

Fig. 5. Part (a): Cu K-edge XANES spectra of Cu-UiO-67-10%bpy in interaction with CO (CO 40%/N_2 gas flow) at RT (dark blue line) and after CO desorption at 523 K in N_2 flux (light blue line). The spectrum of the sample thermally-treated in N_2, collected at RT before CO dosage, is also reported for comparison (red line). Parts (b, c): moduli (b) and imaginary parts (c) of the k^2-weighted, phase uncorrected, FT EXAFS spectra for the same experimental conditions reported in part (a), using the same color code. (For interpretation of the references to color in this figure legend, the reader is referred to the web version of this article.)

reasonable values. From EXAFS analysis, a Cu–C(CO) bond distance of (1.96 ± 0.02) Å is found, in full agreement with the DFT values. Remarkably, the experimentally optimized value is significantly longer with respect to the Cu–O(OH) bond distance determined in the case of four-coordinated Cu(II)(bpydc)(OH)Cl sites in the as-prepared material, (1.91 ± 0.01) Å, see Table 1. The Cu–C(CO) bond distance found here is also longer than that found for Cu(I)$(CO)_2$ and Cu(I)$(CO)_3$ complexes formed inside Cu(I)-ZSM-5 where distances of (1.88 ± 0.02) Å [107] and (1.93 ± 0.02) Å [108], respectively, were observed. The longer distance observed in Cu-UiO-67-10%bpy well agrees with the higher lability of the CO molecule, with respect to the complexes formed in zeolites. The presence of a stronger lig-

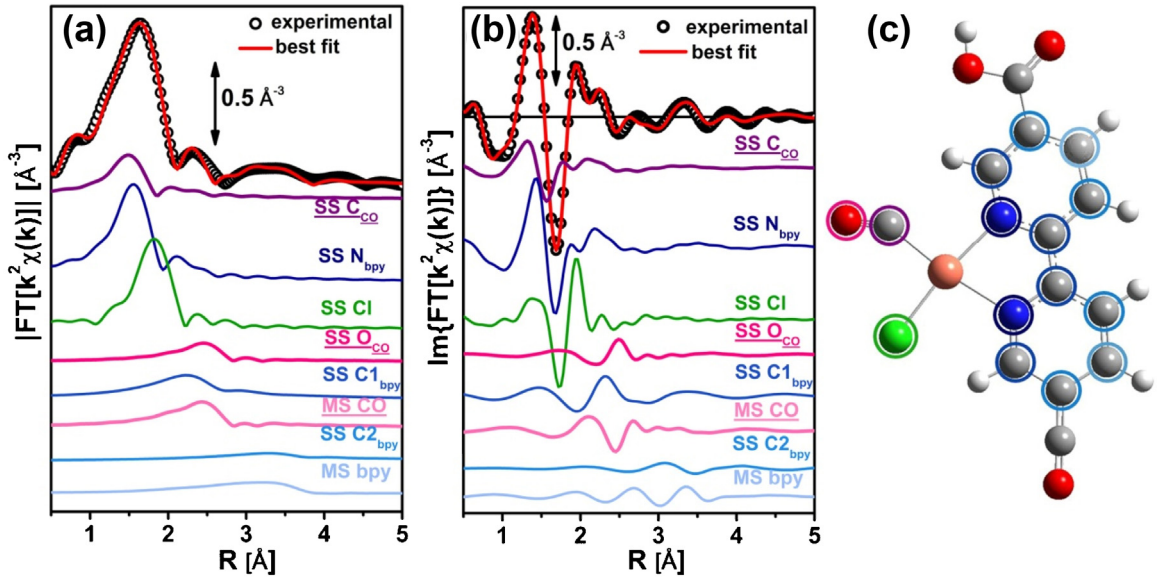

Fig. 6. Part (a): Modulus of the k^2-weighted, phase uncorrected, FT EXAFS spectra for thermally-treated Cu-UiO-67-10%bpy after interaction with CO at RT. The experimental data are shown as scattered black dots and the best fit with red solid lines. Moreover, the single scattering (SS) contribution involving the C(CO), N(bpy), Cl, O(CO), C_1(bpy) and C_2(bpy) atomic neighbors as well as the multiple scattering (MS) involving the atoms of the CO group and of the bpy unit are also reported. Part (b): as part (a) for the imaginary part of the FT. Part (c): DFT-optimized structure used as starting point for the EXAFS fit. Atom color code in part (c): Cu: orange; O: red; N: blue; Cl: green, C: gray; H: white. Circled atoms are those included in the EXAFS fit and the color of the circle is the same used in parts (a, b) for the lines of the corresponding SS paths. (For interpretation of the references to color in this figure legend, the reader is referred to the web version of this article.)

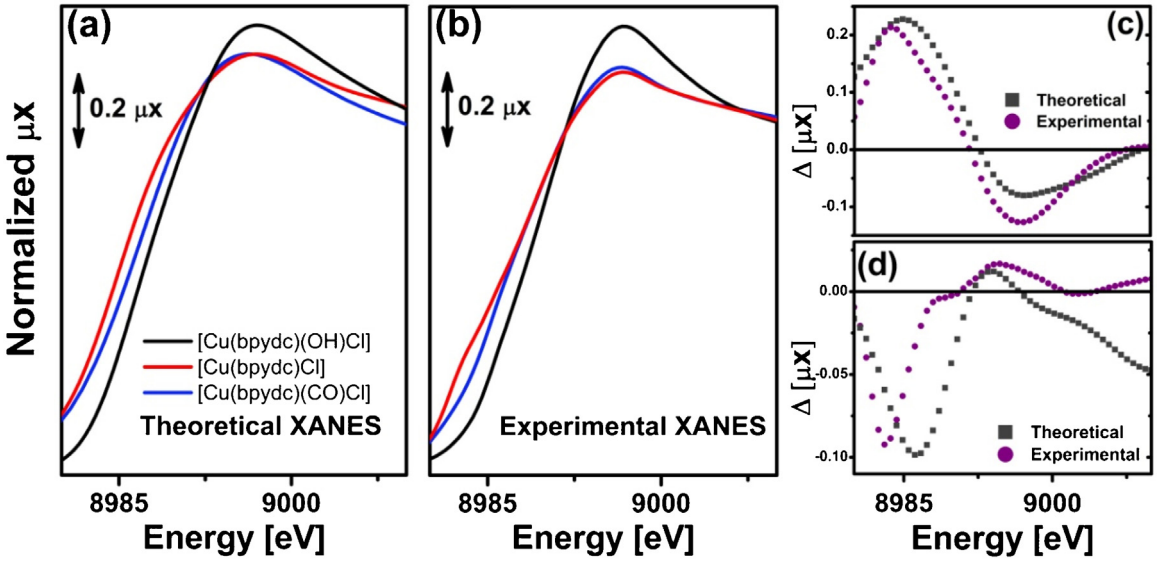

Fig. 7. Part (a): Cu K-edge theoretical XANES spectra calculated with the FDMNES code [87] from DFT-optimized geometries of [Cu(bpydc)(OH)Cl] (black curve), [Cu(bpydc)Cl] (red curve) and [Cu(bpydc)(CO)Cl] (blue curve), representative of the Cu-UiO-67-10%bpy sample in the different experimental conditions. Part (b): as part (a) for the corresponding experimental spectra collected on Cu-UiO-67-10%bpy sample at RT; same color code. Part (c): comparison between the experimental (scattered purple circles) and theoretical (scattered gray squares) difference XANES spectra showing the effect of reduction via thermal treatment: [Cu(bpydc)Cl] – [Cu(bpydc)(OH)Cl]. Part (d): as part (c) for the difference XANES spectra showing the effect of CO adsorption on the thermally-treated sample: [Cu(bpydc)(CO)Cl] – [Cu(bpydc)Cl]. (For interpretation of the references to color in this figure legend, the reader is referred to the web version of this article.)

and as Cl^-, prevents the optimization of the Cu(I)—CO interaction, as well as the formation of di- and tri-carbonyl complexes.

3.5. XANES simulations and discussion on the formal charge on Cu sites

XANES simulations have been performed in order to complement the experimental results reported above, using as input the DFT-optimized geometries for Cu-species identified as the best candidates to reproduce the experimental EXAFS spectra in the different probed conditions. Fig. 7a,b shows the experimental and theoretical XANES spectra for the key states of Cu-UiO-67-10%bpy discussed the previous sections: as-prepared material in air (black), after thermal treatment at 523 K in N_2 (red) and after interaction with CO (blue). Fig. 7a reports the XANES simulations, while Fig. 7b reports the corresponding experimental spectra (all collected at RT), for comparison, drawn with the same color code.

To simulate the spectra we used self-consistent finite-difference method [89], implemented in the accelerated version of the FDMNES software [87,88]. In the three cases, the intensity of

Table 3
Best-fit values of the parameters optimized in the EXAFS fits for the thermally-treated Cu-UiO-67-10%bpy after interaction with CO at RT ($\Delta k = (2.5–12.0)$ Å^{-1}; $\Delta R = (1.0–4.8)$ Å). The underlined parameters were fixed in the fit. DFT-optimized bond distances from the Cu-absorber for the first shell ligands are also reported for comparison in the last column.

EXAFS fit parameters	Thermally-treated Cu-UiO-67-bpy10%+ CO (RT)	DFT-opt. distances [Cu(I)(bpydc)(CO)Cl]
$S_0{}^2$	0.93	–
ΔE (eV)	-2.8 ± 0.4	–
R-factor	0.008	–
N_{par} (N_{ind})	10 (23)	–
$R_{C(CO)}$ (Å)	1.96 ± 0.02	1.96
$\sigma^2{}_{C(CO)}$ (Å^2)	0.0038 ± 0.0002	–
$\sigma^2{}_{MS(CO)}$ (Å^2)	0.005 ± 0.003	–
$<R_{N(bpy)}>$ (Å)	2.025 ± 0.007	2.13
$\sigma^2{}_{N(bpy)}$ (Å^2)	0.0032 ± 0.0008	–
α_{bpy}	-0.042 ± 0.008	–
$\sigma^2{}_{bpy}$ (Å^2)	0.010 ± 0.003	–
R_{Cl} (Å)	2.261 ± 0.006	2.20
$\sigma^2{}_{Cl}$ (Å^2)	0.0041 ± 0.0007	–

the white line well reproduced the changes observed in the experimental spectra. Indeed, the spectrum simulated using the [Cu(bpydc)(OH)Cl] model presents an intense white-line peak, as observed for as-prepared MOFs in air. The white-line peak decreases during thermal treatment in N_2 and it remains almost unchanged upon CO adsorption, as also found in the simulated spectra for [Cu(bpydc)Cl] and [Cu(bpydc)(CO)Cl] models. The energy of the absorption threshold in the simulated spectra qualitatively reproduces the experimental tendency. The position of the threshold obtained for the [Cu(bpydc)(OH)Cl] model is located at higher energy, as observed for the as-prepared MOF in air. Conversely, in the theoretical spectra corresponding to [Cu(bpydc)Cl] and [Cu(bpydc)(CO)Cl] species the absorption threshold shifts at lower energy, in agreement with the experimental evidences for dominant Cu(I) sites after thermal treatment and interaction with CO. The agreement between theory and experiment can be better appreciated in Fig. 7c,d reporting the difference XANES spectra showing the effect of −OH removal and Cu reduction (part c) and of CO adsorption (part d). The difference XANES method (also known as ΔXANES) [109], represents an accurate way to better appreciate small difference in XANES spectra upon small perturbation of the system under investigation. The theory is perfectly able to reproduce the difference observed during the thermal treatment (Fig. 7c), while a less quantitative agreement between theory and experiment is observed upon CO adsorption; however, qualitatively the theory correctly predict a negative $\Delta\mu x$ curve in the (8980–8990) eV range, followed by a positive region, that subsequently decreases in intensity.

The trend of the charge on Cu-site confirmed the results obtained by XANES qualitative analysis and EXAFS fits: the metal starts from a local charge of 1.8 $|e|$ ($\approx$2 $|e|$) for the [Cu(bpydc)(OH)Cl] complex, representative of the as-prepared sample. For the [Cu(bpydc)Cl] complex, modeling the thermally-treated material, the charge on Cu is reduced to 1.1 $|e|$ ($\approx$1 $|e|$). Conversely, the coordination of a CO molecule on Cu(I) sites, [Cu(bpydc)(CO)Cl] model, slightly increases the local charge on Cu to 1.4 $|e|$, although being still significantly lower with respect to what found for the [Cu(bpydc)(OH)Cl] case. The calculated local charge on Cu for the different models qualitatively confirms the experimental observations: Cu(II) centers grafted to the bpydc linker in the as-prepared MOFs, mostly reduced to Cu(I) in N_2 at 523 K. Theoretical modeling suggests that CO coordination leads to a small alteration of local charge around Cu(I), albeit the calculated value of 1.4 $|e|$ is still compatible with a formal +1 oxidation state of the metal centre.

The simulated spectra globally provide a good reproduction of the main experimental XANES features. An improved agreement could be obtained in future studies, considering slight systematic variations from the DFT-minimum of the principal structural parameters, and comparing the resulting theoretical curves with high-energy-resolution XANES data collected at a third-generation source. Furthermore, more sophisticated computational modeling of these materials, considering also the inclusion of the Cu-functionalized bpydc linker in the extended UiO-67 framework, could be envisaged.

3.6. Complementary insights by FTIR spectroscopy

The findings obtained from *in situ* and *operando* XAS were also supported by *in situ* FTIR spectroscopy, which evidenced the coordinative unsaturation of the Cu centers in the thermally-treated materials, able to form the Cu monocarbonyl complexes upon CO adsorption [47,68,108,110,111]. Thermal treatment was followed by *in situ* FTIR measurements at different temperatures, allowing us to monitor the correct desolvation of the MOF, involving the removal from the MOF cavities of residual DMF molecules [112] and H-bonding water from the atmospheric environment (see Fig. 8).

The FTIR spectrum of the as-prepared sample (black curve in Fig. 8a) in the high frequency region (3800–2600 cm^{-1}) is dominated by a complex broad band assigned to the ν(O–H) mode of hydrogen-bonded adsorbed water and to ν(C–H) and ν(C–O) stretching modes of the physisorbed DMF [85,112,113]. Other bands associated to the presence of solvents are evident in the low frequency region. In particular, it is possible to observe signals at 1662 cm^{-1}, at 1256 cm^{-1}, at 1096 cm^{-1} with a shoulder at 1062 cm^{-1} and at 1667 cm^{-1} with a shoulder at 1712 cm^{-1}, assigned to the $\delta(OH_2)$ and $\delta(CH_3)$ modes, respectively. The thermal treatment promotes a significant decrease in the intensity of the bands previously described, according to removal of H_2O and DMF. In particular the spectrum of the sample after thermal treatment at 523 K (red line in Fig. 8) shows the absence of all the bands associated to the DMF and water. It is however worth to note that, differently to what previously reported for not functionalized UiO-66 and UiO-67 [5,6,114], the band at 3676 cm^{-1} associated to the μ_3-OH present at the Zr_6-octahedron do not disappeared completely by heating at 523 K. Unfortunately, the ν(O–H) stretching of [Cu(II)(bpydc)(OH)Cl] species inferred on the basis of the previously discussed DFT-assisted EXAFS fits and XANES simulations, expected around 3657 cm^{-1} [115], could not be confirmed because overshadowed by the huge adsorption of water and DMF molecules present in the channels of the as-prepared material.

As already discussed in the sections devoted to the XAS characterization, the use of a probe molecule like CO allows to get insights on the coordinative unsaturation and reactivity of the Cu sites hosted in the UiO-67 framework. Consequently, we explored by *in situ* FTIR spectroscopy the interaction of the thermally-treated material with CO. It is known that CO is strongly adsorbed at RT on Cu(I) ions since the carbonyls formed are stabilized by back-donation [24,47,68,108,110,111,116–118] while carbonyl species can be formed on Cu(II) only at low temperature [119,120] and are characterized by a very low adsorption enthalpy. For these reasons, carbon monoxide was used as a probe molecule at ~100 K to investigate the nature of copper sites in Cu-UiO-67-bpy after thermal treatment. Measurements were performed on a thin self-supporting wafer of the samples by using cryogenic FTIR cell and the experimental setup described in Section 2.6 to perform *in situ* thermal treatment and controlled gas dosage. Spectra were recorded in the same conditions. At 100 K, carbon monoxide probed a rather heterogeneous population of adsorption sites, as documented by the complex spectra reported in Fig. 9, see in particular the inset, reporting a magnification in the ν(C–O) stretching region.

Three well-defined signals are identified at 2095 cm^{-1}, 2135 cm^{-1} and at 2152 cm^{-1} and a broad tailed absorption in

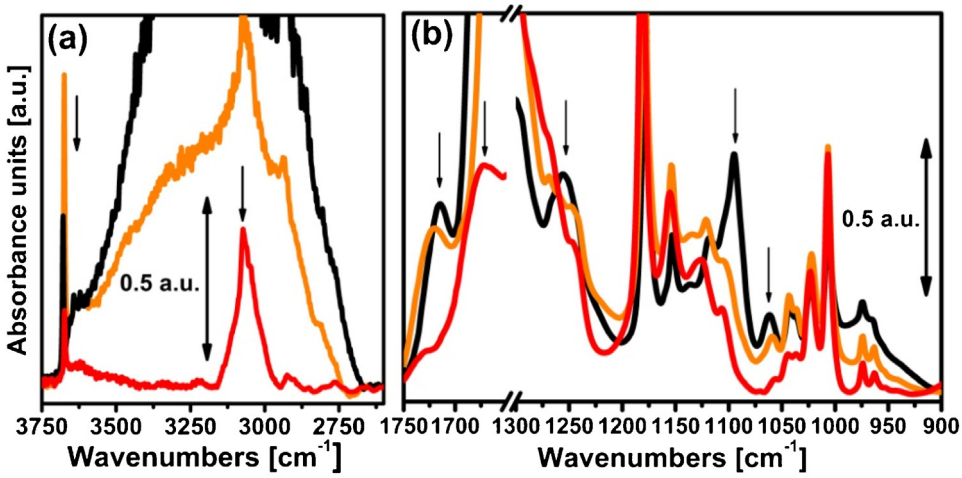

Fig. 8. FTIR spectra of Cu-UiO-67-10%bpy collected at RT on the as-prepared sample (black line), sample heated at an intermediate temperature of 393 K (orange line) and sample after thermal treatment at 523 K (red line), separately shown in the high-frequency, part (a), and low frequency region, part (b). (For interpretation of the references to color in this figure legend, the reader is referred to the web version of this article.)

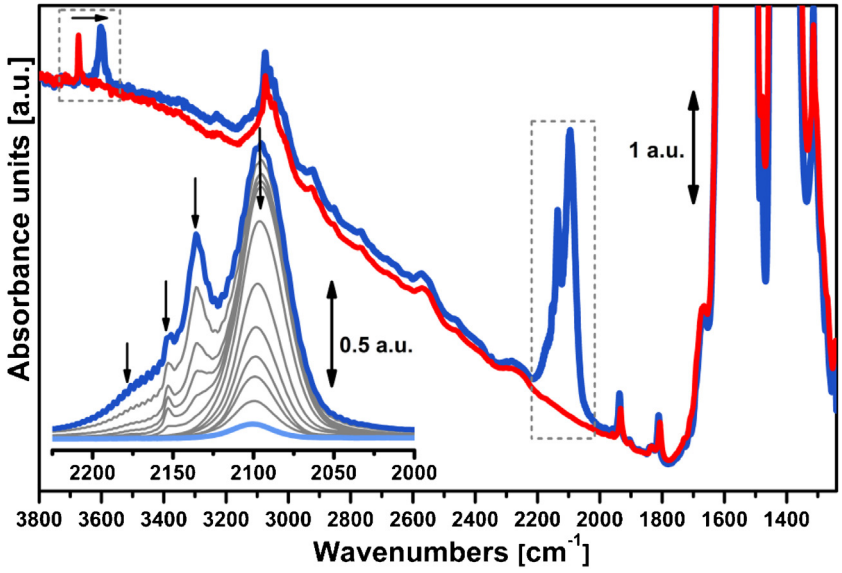

Fig. 9. *In situ* FTIR spectra of Cu-UiO-67-10%bpy collected at RT after thermal treatment at 523 K (red line), and after maximum CO adsorption at 100 K (blue line). The inset shows *in situ* FTIR spectra collected while outgassing CO from maximum (blue line) to minimum (light blue line) coverage; grey thin lines correspond to intermediate CO coverages. (For interpretation of the references to color in this figure legend, the reader is referred to the web version of this article.)

the (2160–2200) cm^{-1} range. All the components are substantially reversible, as testified by the sequence of spectra illustrated in the inset of Fig. 9 (background-subtracted spectra collected during progressive outgassing at 100 K), although with a different relative stability.

On the basis of frequency position, $\Delta\tilde{\nu}^{exp}(CO) = [\tilde{\nu}^{exp}(CO) - \tilde{\nu}_0^{exp}(CO)] = -48\ cm^{-1}$, the dominant band at 2095 cm^{-1} (very intense, symmetric and quite broad) is assigned to the formation of monocarbonyl [Cu(bpydc)(CO)Cl] species with reduced copper species, in good agreement with XAS evidences discussed the previous sections. In case of isolated Cu(I) species hosted as counter ions in zeolites, the appearance of a typical band in the range (2154–2159) cm^{-1} has been assigned to the formation of monocarbonyl Cu(I)(CO) complexes [24,110,115,118]. The higher frequency of Cu(I) carbonyls formed in zeolites was justified by a very high electrostatic contribution due by Cu(I) cations exhibiting a high coordinative unsaturation. In the present case the presence of the negatively charged large Cl^- ligand inhibits the electrostatic part of the cation-CO interaction, lowering the (C–O). Looking in the literature to other Cu(I) carbonyl complexes, it is worth recalling that a band around 2127 cm^{-1} was observed dosing CO on high surface area Cu_2O crystals [121,122]. The carbonyl band observed on highly dispersed CuCl crystals occurs at 2134 cm^{-1} [55,116] the addition of alkaline cation in the salt moves the ν(CO) stretching frequency downwards to 2122 cm^{-1} for Cu_xK_yCl and to 2115 cm^{-1} for Cu_xCs_yCl [123]. We note that in all Cu(I) cases reported above, corresponding carbonyls show a very high stability and they are not reversible upon outgassing at room temperature. Conversely, in the present case, despite to an even lower frequency (below 2100 cm^{-1}) the formation of the carbonyl is nearly totally reversible upon *ca.* 30 min outgassing at 100 K. This peculiar behaviour could be tentatively explained by considering the presence, in the first coordination sphere of the copper sites, of the electron rich Cl and N species, resulting in a "less charged" copper species. For CO adsorbed on Cu(0) metal surfaces different, coverage depended ν(CO) were observed with surface science techniques, depend-

ing on the exposed Cu(*hkl*) face: (2079 – 2088) cm^{-1} on Cu(100) [124]; 2072 cm^{-1} on Cu(111) [125]; (2088 – 2094) cm^{-1} on Cu(110) [126]; (2095 – 2110) cm^{-1} on Cu(211) [127]; (2093 – 2104) cm^{-1} on Cu(311) [127] (when an interval is reported, the first value refers to the lowest coverage, the second value refers to the maximum coverage). However, in the present case the presence of Cu(0) metal nanoparticles is ruled out by our EXAFS study. Comparison with literature data allows us to conclude that the [Cu(bpydc)(CO)Cl] carbonyl formed in functionalized Cu-UiO-67-bpy MOF are electron rich species. DFT simulations qualitatively agree with the experiment in predicting a red shift for the [Cu(bpydc)(CO)Cl] complex, resulting in $\Delta\tilde{\nu}^{theo}(CO) = [\tilde{\nu}^{theo}(CO) - \tilde{\nu}_0^{theo}(CO)] = -24\,cm^{-1}$, but underestimate the shift by 50%.

Together with the main band discussed before, two additional features can be evidenced in the FTIR spectra reported in the inset of Fig. 9. First, we observed a band at 2152 cm^{-1}, slightly blue-shifted with respect to the liquid like, which decreased concomitantly to the restoration of the bands at 3600 cm^{-1}. These evidences allowed us to assign the 2152 cm^{-1} band to an interaction of CO with the residual OH group still present on some Zr–O cornerstones [5,6,114]. The most reversible band is that observed at 2135 cm^{-1}, easily assigned to liquid-like CO [128–130]. This feature is associated with two broad lateral bands due to the rotovibrational profile. The low-frequency tail cannot be observed, since it is totally overshadowed by the much stronger band at 2095 cm^{-1}, while the high-frequency tail corresponds to the previously mentioned broad absorption in the (2160–2200) cm^{-1} range. Behind such broad tail, a small inflection is observed in the highest coverage spectrum revealing the possible presence of a band around 2180 cm^{-1}, expected for Cu(II)–CO adducts [119,120]. Consequently, we cannot exclude the presence of a small fraction of residual Cu(II)-complexes, most likely [Cu(II)(bpydc)(OH)Cl] species, still present as a minor structural component in the material after thermal treatment at 523 K that could result in [Cu(II)(bpydc)(CO)(OH)Cl] adducts upon CO dosage. It is however clear that we are debating about a very minor fraction of copper species.

– Conclusions

The combination of XAS and FTIR spectroscopies, applied under *in situ* and *operando* conditions, allowed us to verify the successful incorporation of Cu ions in the UiO-67 framework in a series of bpydc-containing UiO-67 MOFs, characterized by different percentages of chelating bpydc linkers. Exploiting the element selectivity of XAS, we probed the local environment and oxidation state of Cu sites in the as-prepared material, and monitored its evolution upon mild thermal treatment in N_2-flux at 523 K and after interaction with CO at room temperature.

For the whole samples series, we observed in all the investigated conditions isolated Cu-sites grafted to the MOF framework *via* coordination to the two N atoms of the bpydc unit, without any evidence of metal clusters formation. On the basis of DFT-assisted EXAFS fitting, we identified the other ligands in the Cu-coordination sphere, while tracking by XANES the oxidation state of the Cu centers. In particular, XAS data for the as-prepared materials (collected at room temperature in air) are consistent with a majority of [Cu(II)(bpydc)(OH)Cl] species. The negatively-charged OH^- group is then preferentially released upon heating at 523 K in N_2-flux, triggering a reduction effect of the original four-coordinated Cu(II) sites to three-coordinated Cu(I) species, [Cu(I)(bpydc)Cl], while preserving coordination to the UiO-67 framework by the chelating bpydc linker and, as testified by parallel *in situ* FTIR experiments, the overall MOF structure.

Further insights in the nature and reactivity of these [Cu(I)(bpydc)Cl] complexes, representing an interesting platform for future experiments on Cu(I)-catalyzed reactions, were achieved by monitoring with XAS and FTIR the interaction of the thermally-treated material with the CO probe molecule. Both the techniques pointed out the efficient and reversible formation Cu(I)-mono-carbonyl adducts with CO, compatible with a majority of [Cu(I)(bpydc)(CO)Cl] species as highlighted by EXAFS fitting.

The overall picture is confirmed by XANES simulations for the key experimental conditions investigated, including as-prepared MOFs in air, after thermal treatment in N_2-flux and upon interaction with CO at room temperature.

These results lay the foundations for future *operando* studies aiming to characterize in more detail the redox behavior of the grafted Cu-sites, by exposing the thermally-treated samples to both reducing (*e.g.* H_2 flux), and oxidizing conditions (*e.g.* O_2 flux).

Acknowledgments

C. Lamberti, A. V. Soldatov and L. Braglia acknowledge the Megagrant of the Russian Federation Government to support scientific research at the Southern Federal University, no. 14.Y26.31.0001. K.A. Lomachenko acknowledges the scholarship of the President of Russian Federation for PhD students and young scientists no. СП-2796.2016.1 and the support from the Russian Foundation for Basic Research, project no. 16-32-00572 мол_а. Authors are grateful to MAX-lab for the allocation of the beam time (proposal 20140449) and to Dr. Stefan Carlson for the technical support during the experiments at the I811 beamline.

Appendix A. Supplementary data

Supplementary data associated with this article can be found, in the online version, at http://dx.doi.org/10.1016/j.cattod.2016.02.039.

References

[1] G. Ferey, Chem. Soc. Rev. 37 (2008) 191.
[2] V.V. Butova, M.A. Soldatov, A.A. Guda, K.A. Lomachenko, C. Lamberti, Russ. Chem. Rev. 85 (2016) 280.
[3] J.R. Long, O.M. Yaghi, Chem. Soc. Rev. 38 (2009) 1213.
[4] J.H. Cavka, S. Jakobsen, U. Olsbye, N. Guillou, C. Lamberti, S. Bordiga, K.P. Lillerud, J. Am. Chem. Soc. 130 (2008) 13850.
[5] L. Valenzano, B. Civalleri, S. Chavan, S. Bordiga, M.H. Nilsen, S. Jakobsen, K.P. Lillerud, C. Lamberti, Chem. Mater. 23 (2011) 1700.
[6] S. Chavan, J.G. Vitillo, D. Gianolio, O. Zavorotynska, B. Civalleri, S. Jakobsen, M.H. Nilsen, L. Valenzano, C. Lamberti, K.P. Lillerud, S. Bordiga, Phys. Chem. Chem. Phys. 14 (2012) 1614.
[7] S. Jakobsen, D. Gianolio, D.S. Wragg, M.H. Nilsen, H. Emerich, S. Bordiga, C. Lamberti, U. Olsbye, M. Tilset, K.P. Lillerud, Phys. Rev. B 86 (2012) (Art. n. 125429).
[8] G.C. Shearer, S. Chavan, J. Ethiraj, J.G. Vitillo, S. Svelle, U. Olsbye, C. Lamberti, S. Bordiga, K.P. Lillerud, Chem. Mater. 26 (2014) 4068.
[9] S. Øien, D. Wragg, H. Reinsch, S. Svelle, S. Bordiga, C. Lamberti, K.P. Lillerud, Cryst. Growth Des. 14 (2014) 5370.
[10] A. Corma, H. Garcia, F. Xamena, Chem. Rev. 110 (2010) 4606.
[11] U. Diaz, M. Boronat, A. Corma, Proc. R. Soc. A-Math. Phys. Eng. Sci. 468 (2012) 1927.
[12] J.D. Evans, C.J. Sumby, C.J. Doonan, Chem. Soc. Rev. 43 (2014) 5933.
[13] A. Corma, M. Iglesias, F. Xamena, F. Sanchez, Chem.-Eur. J. 16 (2010) 9789.
[14] K.K. Tanabe, S.M. Cohen, Inorg. Chem. 49 (2010) 6766.
[15] J. Vaclavik, M. Servalli, C. Lothschutz, J. Szlachetko, M. Ranocchiari, J.A. van Bokhoven, ChemCatChem 5 (2013) 692.
[16] W.M. Bloch, A. Burgun, C.J. Coghlan, R. Lee, M.L. Coote, C.J. Doonan, C.J. Sumby, Nat. Chem. 6 (2014) 906.
[17] S. Chavan, J.G. Vitillo, M.J. Uddin, F. Bonino, C. Lamberti, E. Groppo, K.P. Lillerud, S. Bordiga, Chem. Mater. 22 (2010) 4602.
[18] M. Kandiah, M.H. Nilsen, S. Usseglio, S. Jakobsen, U. Olsbye, M. Tilset, C. Larabi, E.A. Quadrelli, F. Bonino, K.P. Lillerud, Chem. Mater. 22 (2010) 6632.
[19] M. Kandiah, S. Usseglio, S. Svelle, U. Olsbye, K.P. Lillerud, M. Tilset, J. Mater. Chem. 20 (2010) 9848.

[20] S. Øien, G. Agostini, S. Svelle, E. Borfecchia, K.A. Lomachenko, L. Mino, E. Gallo, S. Bordiga, U. Olsbye, K.P. Lillerud, C. Lamberti, Chem. Mater. 27 (2015) 1042.
[21] I. Luz, F.X. Llabrés i Xamena, A. Corma, J. Catal. 276 (2010) 134.
[22] L.Y. Liang, D. Astruc, Coord. Chem. Rev. 255 (2011) 2933.
[23] M. Iwamoto, H. Yahiro, Y. Torikai, T. Yoshioka, N. Mizuno, Chem. Lett. 19 (1990) 1967.
[24] C. Lamberti, S. Bordiga, M. Salvalaggio, G. Spoto, A. Zecchina, F. Geobaldo, G. Vlaic, M. Bellatreccia, J. Phys. Chem. B 101 (1997) 344.
[25] C. Lamberti, S. Bordiga, A. Zecchina, M. Salvalaggio, F. Geobaldo, C. Otero Areán, J. Chem. Soc. Faraday Trans. 94 (1998) 1519.
[26] C. Prestipino, G. Berlier, F.X. Llabrés i Xamena, G. Spoto, S. Bordiga, A. Zecchina, G.T. Palomino, T. Yamamoto, C. Lamberti, Chem. Phys. Lett. 363 (2002) 389.
[27] M.H. Groothaert, P.J. Smeets, B.F. Sels, P.A. Jacobs, R.A. Schoonheydt, J. Am. Chem. Soc. 127 (2005) 1394.
[28] J.S. Woertink, P.J. Smeets, M.H. Groothaert, M.A. Vance, B.F. Sels, R.A. Schoonheydt, E.I. Solomon, Proc. Natl. Acad. Sci. U. S. A. 106 (2009) 18908.
[29] P. Vanelderen, J. Vancauwenbergh, B.F. Sels, R.A. Schoonheydt, Coord. Chem. Rev. 257 (2013) 483.
[30] E.M. Alayon, M. Nachtegaal, M. Ranocchiari, J.A. van Bokhoven, Chem. Commun. 48 (2012) 404.
[31] E.M.C. Alayon, M. Nachtegaal, A. Bodi, M. Ranocchiari, J.A. van Bokhoven, Phys. Chem. Chem. Phys. 17 (2015) 7681.
[32] E.M.C. Alayon, M. Nachtegaal, A. Bodi, J.A. van Bokhoven, ACS Catal. 4 (2014) 16.
[33] M.J. Wulfers, S. Teketel, B. Ipek, R.F. Lobo, Chem. Commun. 51 (2015) 4447.
[34] S. Brandenberger, O. Krocher, A. Tissler, R. Althoff, Catal. Rev. 50 (2008) 492.
[35] P. Granger, V.I. Parvulescu, Chem. Rev. 111 (2011) 3155.
[36] U. Deka, I. Lezcano-Gonzalez, B.M. Weckhuysen, A.M. Beale, ACS Catal. 3 (2013) 413.
[37] F. Gao, J. Kwak, J. Szanyi, C.F. Peden, Top. Catal. 56 (2013) 1441.
[38] A.M. Beale, F. Gao, I. Lezcano-Gonzalez, C.H.F. Peden, J. Szanyi, Chem. Soc. Rev. 44 (2015) 7371.
[39] F. Giordanino, E. Borfecchia, K.A. Lomachenko, A. Lazzarini, G. Agostini, E. Gallo, A.V. Soldatov, P. Beato, S. Bordiga, C. Lamberti, J. Phys. Chem. Lett. 5 (2014) 1552.
[40] E. Borfecchia, K.A. Lomachenko, F. Giordanino, H. Falsig, P. Beato, A.V. Soldatov, S. Bordiga, C. Lamberti, Chem. Sci. 6 (2015) 548.
[41] T.V.W. Janssens, H. Falsig, L.F. Lundegaard, P.N.R. Vennestrøm, S.B. Rasmussen, P.G. Moses, F. Giordanino, E. Borfecchia, K.A. Lomachenko, C. Lamberti, S. Bordiga, A. Godiksen, S. Mossin, P. Beato, ACS Catal. 5 (2015) 2832.
[42] R.J. Quinlan, M.D. Sweeney, L. Lo Leggio, H. Otten, J.C.N. Poulsen, K.S. Johansen, K. Krogh, C.I. Jorgensen, M. Tovborg, A. Anthonsen, T. Tryfona, C.P. Walter, P. Dupree, F. Xu, G.J. Davies, P.H. Walton, Proc. Natl. Acad. Sci. U. S. A. 108 (2011) 15079.
[43] G. Vaaje-Kolstad, B. Westereng, S.J. Horn, Z.L. Liu, H. Zhai, M. Sorlie, V.G.H. Eijsink, Science 330 (2010) 219.
[44] C.H. Kjaergaard, M.F. Qayyum, S.D. Wong, F. Xu, G.R. Hemsworth, D.J. Walton, N.A. Young, G.J. Davies, P.H. Walton, K.S. Johansen, K.O. Hodgson, B. Hedman, E.I. Solomon, Proc. Natl. Acad. Sci. U. S. A. 111 (2014) 8797.
[45] G. Ferey, Chem. Mater. 13 (2001) 3084.
[46] M. Eddaoudi, D.B. Moler, H.L. Li, B.L. Chen, T.M. Reineke, M. O'Keeffe, O.M. Yaghi, Acc. Chem. Res. 34 (2001) 319.
[47] E. Groppo, M.J. Uddin, S. Bordiga, A. Zecchina, C. Lamberti, Angew. Chem.-Int. Ed. 47 (2008) 9269.
[48] Y. Sato, M. Kagotani, T. Yamamoto, Y. Souma, Appl. Catal. A-Gen. 185 (1999) 219.
[49] Y. Sato, M. Kagotani, Y. Souma, J. Mol. Catal. A-Chem. 151 (2000) 79.
[50] Y. Sato, T. Yamamoto, Y. Souma, Catal. Lett. 65 (2000) 123.
[51] H.C. Meinders, G. Challa, J. Mol. Catal. 7 (1980) 321.
[52] R.G. Tailleur, C.J.G. Garcia, J. Catal. 250 (2007) 110.
[53] G. Leofanti, M. Padovan, M. Garilli, D. Carmello, A. Zecchina, G. Spoto, S. Bordiga, G.T. Palomino, C. Lamberti, J. Catal. 189 (2000) 91.
[54] G. Leofanti, M. Padovan, M. Garilli, D. Carmello, G.L. Marra, A. Zecchina, G. Spoto, S. Bordiga, C. Lamberti, J. Catal. 189 (2000) 105.
[55] G. Leofanti, A. Marsella, B. Cremaschi, M. Garilli, A. Zecchina, G. Spoto, S. Bordiga, P. Fisicaro, G. Berlier, C. Prestipino, G. Casali, C. Lamberti, J. Catal. 202 (2001) 279.
[56] G. Leofanti, A. Marsella, B. Cremaschi, M. Garilli, A. Zecchina, G. Spoto, S. Bordiga, P. Fisicaro, C. Prestipino, F. Villain, C. Lamberti, J. Catal. 205 (2002) 375.
[57] C. Lamberti, C. Prestipino, F. Bonino, L. Capello, S. Bordiga, G. Spoto, A. Zecchina, S.D. Moreno, B. Cremaschi, M. Garilli, A. Marsella, D. Carmello, S. Vidotto, G. Leofanti, Angew. Chem.-Int. Ed. 41 (2002) 2341.
[58] N.B. Muddada, U. Olsbye, L. Caccialupi, F. Cavani, G. Leofanti, D. Gianolio, S. Bordiga, C. Lamberti, Phys. Chem. Chem. Phys. 12 (2010) 5605.
[59] N.B. Muddada, U. Olsbye, G. Leofanti, D. Gianolio, F. Bonino, S. Bordiga, T. Fuglerud, S. Vidotto, A. Marsella, C. Lamberti, Dalton Trans. 39 (2010) 8437.
[60] N.B. Muddada, T. Fuglerud, C. Lamberti, U. Olsbye, Top. Catal. 57 (2014) 741.
[61] G.A. Ozin, C. Gil, Chem. Rev. 89 (1989) 1749.
[62] S. Kitagawa, R. Matsuda, Coord. Chem. Rev. 251 (2007) 2490.
[63] S.H. Cho, B.Q. Ma, S.T. Nguyen, J.T. Hupp, T.E. Albrecht-Schmitt, Chem. Commun. (2006) 2563.
[64] J. Singh, C. Lamberti, J.A. van Bokhoven, Chem. Soc. Rev. 39 (2010) 4754.
[65] S. Bordiga, F. Bonino, K.P. Lillerud, C. Lamberti, Chem. Soc. Rev. 39 (2010) 4885.
[66] S. Bordiga, E. Groppo, G. Agostini, J.A. van Bokhoven, C. Lamberti, Chem. Rev. 113 (2013) 1736.
[67] C. Garino, E. Borfecchia, R. Gobetto, J.A. van Bokhoven, C. Lamberti, Coord. Chem. Rev. 277 (2014) 130.
[68] S. Bordiga, C. Lamberti, F. Bonino, A. Travert, F. Thibault-Starzyk, Chem. Soc. Rev. 44 (2015) 7262.
[69] C. Lamberti, J.A. van Bokhoven, X-ray absorption and emission spectroscopy for catalysis, in: J.A. van Bokhoven, C. Lamberti (Eds.), X-Ray Absorption and X-Ray Emission Spectroscopy: Theory and Applications, John Wiley & Sons, Chichester, 2016, p. 353.
[70] A. Schaate, P. Roy, A. Godt, J. Lippke, F. Waltz, M. Wiebcke, P. Behrens, Chem.-Eur. J. 17 (2011) 6643.
[71] D.J. Awad, U. Schilde, P. Strauch, Inorg. Chim. Acta 365 (2011) 127.
[72] B. Spingler, S. Schnidrig, T. Todorova, F. Wild, CrystEngComm 14 (2012) 751.
[73] S. Carlson, M. Clausen, L. Gridneva, B. Sommarin, C. Svensson, J. Synchrot. Radiat. 13 (2006) 359.
[74] C. Lamberti, C. Prestipino, S. Bordiga, G. Berlier, G. Spoto, A. Zecchina, A. Laloni, F. La Manna, F. D'Anca, R. Felici, F. D'Acapito, P. Roy, Nucl. Instrum. Methods Phys. Res. Sect. B-Beam Interact. Mater. Atoms 200 (2003) 196.
[75] B. Ravel, M. Newville, J. Synchrotron Radiat. 12 (2005) 537.
[76] J.P. Perdew, K. Burke, M. Ernzerhof, Phys. Rev. Lett. 77 (1996) 3865.
[77] G. Kresse, J. Furthmuller, Comput. Mater. Sci. 6 (1996) 15.
[78] G. Kresse, J. Furthmuller, Phys. Rev. B 54 (1996) 11169.
[79] O.R. Gilliam, C.M. Johnson, W. Gordy, Phys. Rev. 78 (1950) 140.
[80] G.E. Ewing, J. Chem. Phys. 37 (1962) 2250.
[81] S.I. Zabinsky, J.J. Rehr, A. Ankudinov, R.C. Albers, M.J. Eller, Phys. Rev. B 52 (1995) 2995.
[82] J.J. Rehr, R.C. Albers, Rev. Mod. Phys. 72 (2000) 621.
[83] E. Groppo, C. Prestipino, C. Lamberti, P. Luches, C. Giovanardi, F. Boscherini, J. Phys. Chem. B 107 (2003) 4597.
[84] C. Lamberti, E. Groppo, C. Prestipino, S. Casassa, A.M. Ferrari, C. Pisani, C. Giovanardi, P. Luches, S. Valeri, F. Boscherini, Phys. Rev. Lett. 91 (2003) (Art. n. 046101).
[85] F. Bonino, S. Chavan, J.G. Vitillo, E. Groppo, G. Agostini, C. Lamberti, P.D.C. Dietzel, C. Prestipino, S. Bordiga, Chem. Mater. 20 (2008) 4957.
[86] E. Borfecchia, S. Maurelli, D. Gianolio, E. Groppo, M. Chiesa, F. Bonino, C. Lamberti, J. Phys. Chem. C 116 (2012) 19839.
[87] S.A. Guda, A.A. Guda, M.A. Soldatov, K.A. Lomachenko, A.L. Bugaev, C. Lamberti, W. Gawelda, C. Bressler, G. Smolentsev, A.V. Soldatov, Y. Joly, J. Chem. Theory Comput. 11 (2015) 4512.
[88] Y. Joly, Phys. Rev. B 63 (2001) (Art. n. 125120).
[89] O. Bunau, Y. Joly, J. Phys.-Condens. Matter 21 (2009) (Art. n. 345501).
[90] K.A. Lomachenko, C. Garino, E. Gallo, D. Gianolio, R. Gobetto, P. Glatzel, N. Smolentsev, G. Smolentsev, A.V. Soldatov, C. Lamberti, L. Salassa, Phys. Chem. Chem. Phys. 15 (2013) 16152.
[91] C. Deiana, M. Minella, G. Tabacchi, V. Maurino, E. Fois, G. Martra, Phys. Chem. Chem. Phys. 15 (2013) 307.
[92] G.M. Sheldrick, Acta Crystallogr. Sect. C-Struct. Chem. 71 (2015) 3.
[93] O.V. Dolomanov, L.J. Bourhis, R.J. Gildea, J.A.K. Howard, H. Puschmann, J. Appl. Crystallogr. 42 (2009) 339.
[94] H. Putz, K. Brandenburg, Diamond–Crystal and Molecular Structure Visualization Ver. 4.1.2, Crystal Impact, Bonn, Germany, 1997.
[95] F.H. Allen, O. Johnson, G.P. Shields, B.R. Smith, M. Towler, J. Appl. Crystallogr. 37 (2004) 335.
[96] S. Øien, D.S. Wragg, K.P. Lillerud, M. Tilset, Acta Cryst. E 69 (2013) m73.
[97] G. Turnes Palomino, P. Fisicaro, S. Bordiga, A. Zecchina, E. Giamello, C. Lamberti, J. Phys. Chem. B 104 (2000) 4064.
[98] F.X. Llabrés i Xamena, P. Fisicaro, G. Berlier, A. Zecchina, G. Turnes Palomino, C. Prestipino, S. Bordiga, E. Giamello, C. Lamberti, J. Phys. Chem. B 107 (2003) 7036.
[99] M. Benfatto, P. D'Angelo, S. Della Longa, N.V. Pavel, Phys. Rev. B 65 (2002) (Art. n 174205).
[100] L.S. Kau, D.J. Spirasolomon, J.E. Pennerhahn, K.O. Hodgson, E.I. Solomon, J. Am. Chem. Soc. 109 (1987) 6433.
[101] M.H. Groothaert, J.A. van Bokhoven, A.A. Battiston, B.M. Weckhuysen, R.A. Schoonheydt, J. Am. Chem. Soc. 125 (2003) 7629.
[102] C. Lamberti, S. Bordiga, F. Bonino, C. Prestipino, G. Berlier, L. Capello, F. D'Acapito, F. Xamena, A. Zecchina, Phys. Chem. Chem. Phys. 5 (2003) 4502.
[103] M. Sano, S. Komorita, H. Yamatera, Inorg. Chem. 31 (1992) 459.
[104] L. Salassa, C. Garino, G. Salassa, C. Nervi, R. Gobetto, C. Lamberti, D. Gianolio, R. Bizzarri, P.J. Sadler, Inorg. Chem. 48 (2009) 1469.
[105] L. Salassa, T. Ruiu, C. Garino, A.M. Pizarro, F. Bardelli, D. Gianolio, A. Westendorf, P.J. Bednarski, C. Lamberti, R. Gobetto, P.J. Sadler, Organometallics 29 (2010) 6703.
[106] L. Salassa, E. Borfecchia, T. Ruiu, C. Garino, D. Gianolio, R. Gobetto, P.J. Sadler, M. Cammarata, M. Wulff, C. Lamberti, Inorg. Chem. 49 (2010) 11240.
[107] C. Prestipino, L. Capello, F. D'Acapito, C. Lamberti, Phys. Chem. Chem. Phys. 7 (2005) 1743.
[108] C. Lamberti, G.T. Palomino, S. Bordiga, G. Berlier, F. D'Acapito, A. Zecchina, Angew. Chem.-Int. Ed. 39 (2000) 2138.
[109] D.E. Ramaker, Novel XAS techniques for probing fuel cells and batteries, in: J.A. van Bokhoven, C. Lamberti (Eds.), X-Ray Absorption and X-Ray Emission Spectroscopy: Theory and Applications, John Wiley & Sons, Chichester (UK), 2016, p. 485.

[110] V. Bolis, A. Barbaglia, S. Bordiga, C. Lamberti, A. Zecchina, J. Phys. Chem. B 108 (2004) 9970.
[111] C. Lamberti, A. Zecchina, E. Groppo, S. Bordiga, Chem. Soc. Rev. 39 (2010) 4951.
[112] F. Bonino, C. Lamberti, S. Chavan, J.G. Vitillo, S. Bordiga, Characterization of MOFs. 1. Combined vibrational and electronic spectroscopies, in: F.X. Llabrés i Xamena, J. Gascón (Eds.), Metal Organic Frameworks as Heterogeneous Catalysts, The Royal Society of Chemistry, Cambridge, 2013, p. 76.
[113] N. Masciocchi, S. Galli, V. Colombo, A. Maspero, G. Palmisano, B. Seyyedi, C. Lamberti, S. Bordiga, J. Am. Chem. Soc. 132 (2010) 7902.
[114] G.C. Shearer, S. Forselv, S. Chavan, S. Bordiga, K. Mathisen, M. Bjorgen, S. Svelle, K.P. Lillerud, Top. Catal. 56 (2013) 770.
[115] F. Giordanino, P.N.R. Vennestrom, L.F. Lundegaard, F.N. Stappen, S. Mossin, P. Beato, S. Bordiga, C. Lamberti, Dalton Trans. 42 (2013) 12741.
[116] D. Scarano, P. Galletto, C. Lamberti, R. DeFranceschi, A. Zecchina, Surf. Sci. 387 (1997) 236.
[117] A. Zecchina, S. Bordiga, G.T. Palomino, D. Scarano, C. Lamberti, M. Salvalaggio, J. Phys. Chem. B 103 (1999) 3833.
[118] G. Turnes Palomino, S. Bordiga, A. Zecchina, G.L. Marra, C. Lamberti, J. Phys. Chem. B 104 (2000) 8641.
[119] C. Prestipino, L. Regli, J.G. Vitillo, F. Bonino, A. Damin, C. Lamberti, A. Zecchina, P.L. Solari, K.O. Kongshaug, S. Bordiga, Chem. Mater. 18 (2006) 1337.
[120] S. Bordiga, L. Regli, F. Bonino, E. Groppo, C. Lamberti, B. Xiao, P.S. Wheatley, R.E. Morris, A. Zecchina, Phys. Chem. Chem. Phys. 9 (2007) 2676.
[121] D. Scarano, S. Bordiga, C. Lamberti, G. Spoto, G. Ricchiardi, A. Zecchina, C.O. Arean, Surf. Sci. 411 (1998) 272.
[122] S. Bordiga, C. Paze, G. Berlier, D. Scarano, G. Spoto, A. Zecchina, C. Lamberti, Catal. Today 70 (2001) 91.
[123] N.B. Muddada, U. Olsbye, T. Fuglerud, S. Vidotto, A. Marsella, S. Bordiga, D. Gianolio, G. Leofanti, C. Lamberti, J. Catal. 284 (2011) 236.
[124] K. Horn, J. Pritchard, Surf. Sci. 55 (1976) 701.
[125] H. Nishiyama, Y. Inoue, Surf. Sci. 594 (2005) 156.
[126] K. Horn, M. Hussain, J. Pritchard, Surf. Sci. 63 (1977) 244.
[127] J. Pritchard, T. Catterick, R.K. Gupta, Surf. Sci. 53 (1975) 1.
[128] S. Bordiga, E.E. Platero, C.O. Arean, C. Lamberti, A. Zecchina, J. Catal. 137 (1992) 179.
[129] S. Bordiga, D. Scarano, G. Spoto, A. Zecchina, C. Lamberti, C.O. Arean, Vib. Spectrosc. 5 (1993) 69.
[130] C. Lamberti, C. Morterra, S. Bordiga, G. Cerrato, D. Scarano, Vib. Spectrosc. 4 (1993) 273.